

Volcanic perturbations of the marine environment in South China preceding the latest Permian mass extinction and their biotic effects

J. SHEN,¹ T. J. ALGEO,² L. ZHOU,¹ Q. FENG,¹ J. YU³ AND B. ELLWOOD⁴

¹State Key Laboratory of Geological Process and Mineral Resources, China University of Geosciences, Wuhan, Hubei, China

²Department of Geology, University of Cincinnati, Cincinnati, OH, USA

³Laboratory of Biological and Environmental Geology, China University of Geosciences, Wuhan, Hubei, China

⁴Department of Geology and Geophysics, Louisiana State University, Baton Rouge, LA, USA

ABSTRACT

The Dongpan section in southern Guangxi Province records the influence of local volcanic activity on marine sedimentation at intermediate water depths (~200–500 m) in the Nanpanjiang Basin (South China) during the late Permian crisis. We analyzed ~100 samples over a 12-m-thick interval, generating palynological, paleobiological, and geochemical datasets to investigate the nature and causes of environmental changes. The section records at least two major volcanic episodes that culminated in deposition of approximately 25- to 35-cm-thick ash layers (bentonites) and that had profound effects on conditions in both the Dongpan marine environment and adjacent land areas. Intensification of eruptive activity during each volcanic cycle resulted in a shift toward conifer forests, increased wildfire intensity, and elevated subaerial weathering fluxes. The resulting increase in nutrient fluxes stimulated marine productivity in the short term but led to a negative feedback on productivity in the longer term as the OMZ of the Nanpanjiang Basin expanded, putting both phytoplankton and zooplankton communities under severe stress. Radiolarians exhibit large declines in diversity and abundance well before the global mass extinction horizon, demonstrating the diachroneity of the marine biotic crisis. The latest Permian crisis, which was probably triggered by the Siberian Traps flood basalts, intensified the destructive effects of the earlier local eruptions on terrestrial and marine ecosystems of the South China craton.

Received 26 April 2011; accepted 6 October 2011

Corresponding author. Q. Feng. Tel.: +8618971193331; fax: +8602767883002; e-mail: qinglaifeng@cug.edu.cn

INTRODUCTION

The latest Permian mass extinction (LPME) immediately preceding the ~252-Ma Permian–Triassic boundary (PTB) eliminated ~90% of marine species and many terrestrial taxa, making it the largest biotic catastrophe of the Phanerozoic in terms of taxonomic diversity losses (Erwin *et al.*, 2002; Alroy *et al.*, 2008). The pattern and mechanism of extinctions during this crisis are currently the subject of intense research and debate, with some researchers advocating an abrupt, single-phase extinction event (Jin *et al.*, 2000; Rampino *et al.*, 2000) while others proposing a more gradual and/or multiphased crisis (De Wit *et al.*, 2002; Xie *et al.*, 2005; Yin *et al.*, 2007). Most high-resolution chemostratigraphic studies to date have been undertaken on sections representing either shallow-marine environments, especially in the Tethyan realm (Algeo *et al.*, 2007a, 2008; Cao *et al.*, 2009; Luo *et al.*, 2011), or deep-water facies of the Panthal-

assic Ocean (Kato *et al.*, 2002; Takahashi *et al.*, 2009). Recently, however, it has been recognized that the largest changes in oceanic redox conditions during the PTB crisis may have occurred within the oceanic oxygen-minimum zone (OMZ) at intermediate water depths (~100 to 1000 m) (Algeo *et al.*, 2010, 2011a), suggesting that investigations of sections representing deep-shelf settings would be useful. Such sections have a high potential to record relationships among seawater nutrient inventories, primary productivity rates, organic carbon sinking fluxes, and the composition of the marine plankton community (Knoll *et al.*, 2007; Algeo *et al.*, 2011b). A number of deep-shelf sections are known from the Nanpanjiang Basin of the South China craton (e.g. Riccardi *et al.*, 2006; Feng *et al.*, 2007; Isozaki *et al.*, 2007).

The South China craton experienced substantial volcanic activity of regional origin during the Late Permian and Early Triassic (Yin *et al.*, 1992; Tong *et al.*, 2007). The LPME in

the global system stratotype and point (GSSP) section for the PTB at Meishan D in Zhejiang Province (Fig. 1A; Yin *et al.*, 2001, 2007) coincides with an ash layer (Bed 25; Jin *et al.*, 2000), and this layer has been identified from >35 localities in 12 provinces of southern and eastern China (Yin *et al.*, 1992; Peng *et al.*, 2001). Additional ash layers are present at Meishan, and the number and thickness of ash layers in the PTB interval *sensu lato* increase southwestward into Guizhou, Guangxi, and Yunnan provinces, where some sections record dozens of ashfall events (Feng *et al.*, 2007; Xie *et al.*, 2010). These regional eruptions were probably sourced in subduction zones along the western and southern margins of the South China craton (Li, 1998; Yang, 1998) and were unrelated to contemporaneous flood basalt volcanism of the Siberian Traps (Reichow *et al.*, 2009; Xie *et al.*, 2010). The role of regional volcanism in promoting environmental changes in marine ecosystems across South China has not been investigated in detail to date. In this study, we document the effects of regional volcanism on deepwater environments and biotas of the Nanpanjiang Basin immediately preceding the LPME utilizing a high-resolution multiproxy dataset generated from the Dongpan section in southern Guangxi Province.

GEOLOGICAL SETTING AND STRATIGRAPHY

Many marine successions in the South China region provide a continuous record of sedimentation across the PTB (Yang *et al.*, 1987; Feng *et al.*, 2007). In the Nanpanjiang Basin, the Upper Permian consists of two distinct facies representing shallow- and deepwater settings (Fig. 1C). The shallow-water facies consists of fossiliferous wackestones and packstones deposited in carbonate platform settings. The deepwater facies consists of radiolarian cherts and claystones (assigned to the Dalong Formation and its stratigraphic equivalents) that were deposited in slope and basin environments of interplatform troughs. The water depths associated with this facies have been estimated at 200–500 m based on the composition of the radiolarian, brachiopod, and ostracod assemblages (He *et al.*, 2005a, 2007; Yin *et al.*, 2007). Exposures of the Dalong Formation containing well-preserved radiolarian faunas have been reported from Guangxi, Guizhou, and Sichuan provinces in southwestern China (Fig. 1A; Feng *et al.*, 2000; Feng & Gu, 2002; Feng *et al.*, 2007).

The Dongpan section is located at 22°16.196 N and 107°41.505 E, between the villages of Dongmen and Liuqiao

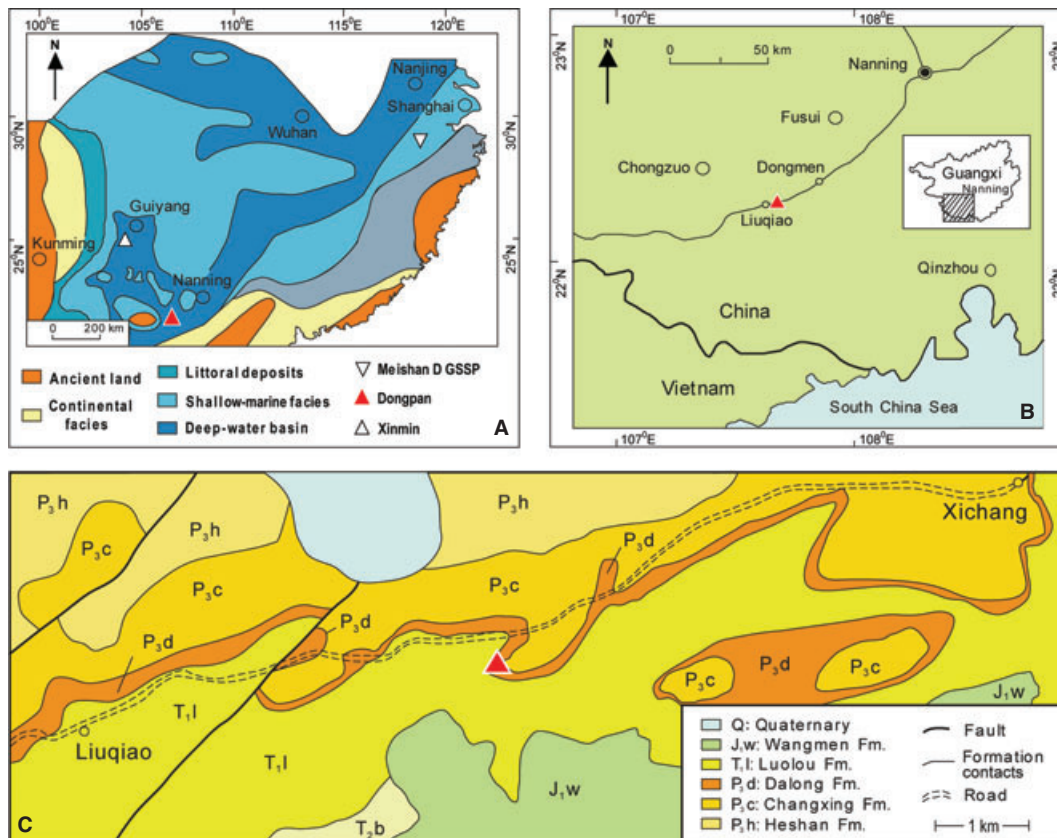


Fig. 1 (A) Paleogeography of South China during the Late Permian to Early Triassic (modified after Feng & Gu, 2002). (B) Location of Dongpan section in southern Guangxi Province. (C) Geology of study area near Liuqiao.

in Fusui County, Guangxi Zhuang Autonomous Region (Fig. 1B). It has been the subject of earlier litho- and biostratigraphic studies (He *et al.*, 2005a, 2007; Meng *et al.*, 2005; Feng *et al.*, 2007; Zhang *et al.*, 2007; Luo *et al.*, 2008) but has not previously been investigated geochemically except for organic $\delta^{13}\text{C}$ (Zhang *et al.*, 2006). The section is of low to moderate thermal maturity, yielding vitrinite reflectances (R_0) of 0.65–1.35 (Li, 1989) and conodont color alteration indices

(CAI) of 2–3 (Luo *et al.*, 2011; G.M. Luo, pers. comm.), which are equivalent to maximum burial temperatures of ~70–120°C (Hunt, 1996, p. 389). It consists of the uppermost 10 m of the Upper Permian Dalong Formation and the lowermost 2 m of the Lower Triassic Luolou Formation (Fig. 2). The lower part (Beds 2–6) is composed mainly of thin-bedded mudstones, siliceous mudstones, and cherts yielding abundant radiolarians, foraminifera, ostracods, and a

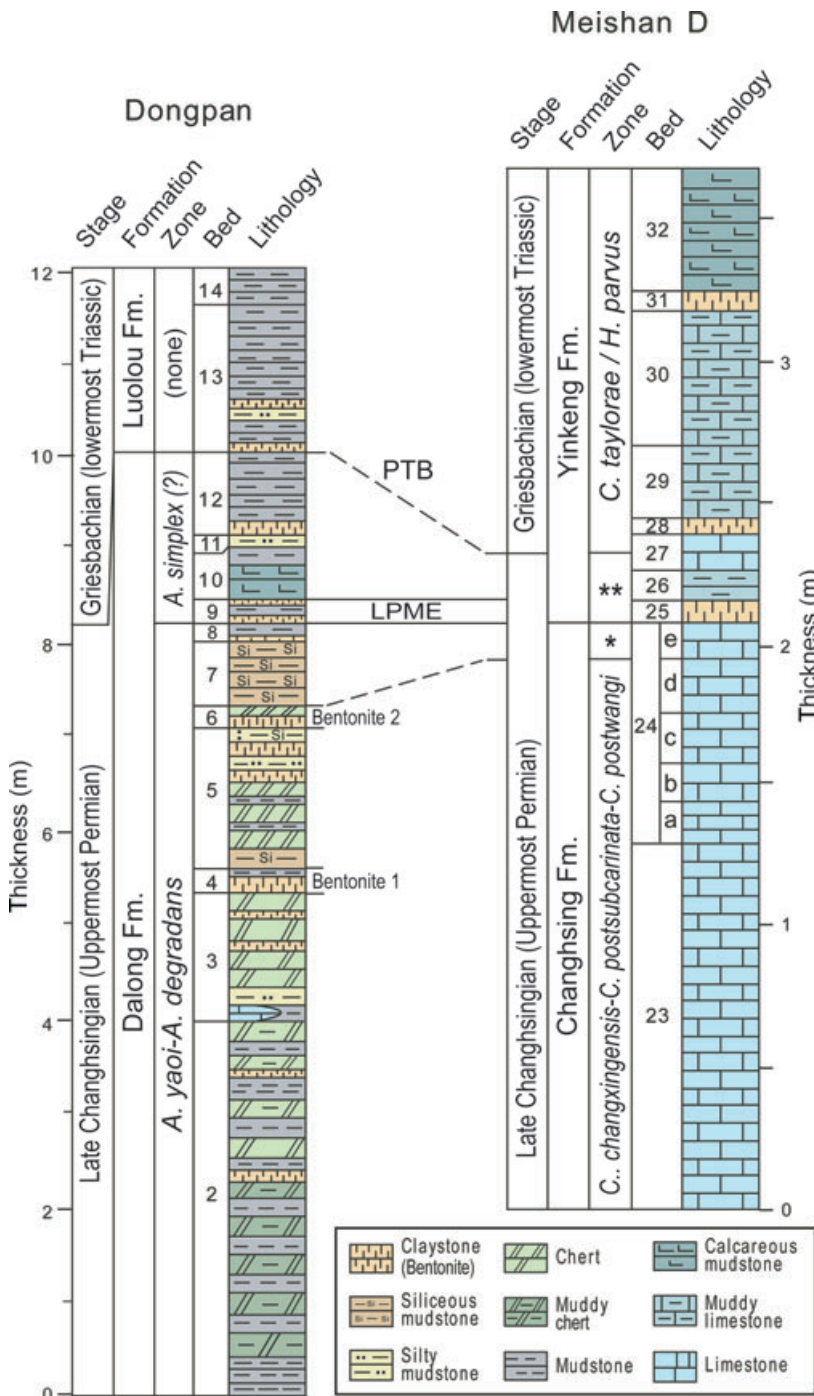


Fig. 2 Lithologic column for Dongpan and correlation with Meishan D GSSP (modified from Feng *et al.*, 2007). The asterisk (*) and double asterisk (**) at Meishan D represent the *C. yini/H. latidentatus* and *C. meishanensis/H. praeparvus* conodont zones, respectively. See text for discussion of correlations.

few ammonites and brachiopods, with interspersed non-fossiliferous claystone interbeds (Feng *et al.*, 2007). The middle part (Beds 7–12) consists of siliceous mudstones with more frequent claystone intercalations and contains a much reduced biota, consisting of small brachiopods, bivalves, and gastropods, as well as some ostracods and radiolarians (He *et al.*, 2005a, 2007). The upper part (Beds 13–14) consists mainly of mudstone with some interspersed claystone beds. The claystone beds have been identified as volcanic ash layers (bentonites) on the basis of their field and petrographic characteristics (Meng *et al.*, 2005; cf. Yin *et al.*, 1992). The two most prominent ash layers, here termed Bentonites 1 and 2 (equivalent to Beds 4 and 6, respectively; Fig. 2), were sampled and geochemically analyzed as part of this study.

The Dongpan section can be correlated with the Meishan D GSSP owing to recent improvements in correlation of deepwater radiolarian-dominated chert facies with shallow-water conodont-bearing carbonate facies. In Japanese sections, most of the Upper Permian Changhsingian stage was assigned previously to the *Neobaiella optima* radiolarian zone (Kuwahara *et al.*, 1998), but Xia *et al.* (2004) subdivided this interval into six zones, of which the youngest three are the *Albaillella yaoi*, *Albaillella degradans*, and *Albaillella simplex* zones, each based on the first appearance of the eponymous taxon. Xia *et al.* (2004) correlated the *yaoi* and *degradans* zones respectively with the *C. changxingensis*, *C. postsubcarinata*, *C. postwangi*, *C. deflecta* and *C. yini/H. latidentatus* conodont zones of late Changhsingian age (both pre-LPME), and the *simplex* zone with the *C. meishanensis/H. praeparvus* conodont zone of latest Changhsingian age (post-LPME, pre-PTB). A limited radiolarian fauna has been recovered from Meishan D, but it is not particularly age-diagnostic (He *et al.*, 2005b).

At Dongpan, Beds 2–5 contain abundant specimens of *A. yaoi* as well as *A. triangularis*, *N. optima*, and many other radiolarian species (Feng *et al.*, 2007). Bed 6 contains only rare specimens of a single *Albaillella* species along with strongly reduced concentrations of other radiolarian orders and represents the main extinction event for radiolarians at Dongpan (Feng *et al.*, 2007). This extinction episode pre-dates the global extinction horizon represented by the LPME (Fig. 2) and has been documented in other sections, for example, by the sharp reduction in radiolarians ~3.5 m below the main marine extinction horizon at Chaotian in South China (Isozaki *et al.*, 2007). Beds 2–6 are thus of late Changhsingian age, corresponding to the *yaoi* zone and possibly the *degradans* zone (n.b., the taxon *A. degradans* was not identified at Dongpan).

Although Beds 7–9 at Dongpan lack diagnostic taxa, the LPME has been placed at the Bed 9/10 contact on the basis of a major decline in brachiopods, foraminifera, and ostracods (He *et al.*, 2007; Yin *et al.*, 2007) and a negative excursion in $\delta^{13}\text{C}_{\text{org}}$ that matches one in Bed 25 at Meishan D (Zhang *et al.*, 2006). The Bed 9 ash layer in the Dongpan section is at the same stratigraphic level as the Bed 25 ash layer at Meishan

and, hence, is likely to represent the same eruptive event (Fig. 2). Beds 10–12 at Dongpan contain only a sparse, depauperate biota lacking diagnostic taxa, but they are inferred to correspond to the *simplex* zone based on stratigraphic position. The base of Bed 13 yielded the Early Triassic ammonoids *Ophiceras* sp. and *Ophiceras tingi* Tien as well the Early Triassic bivalve *Claraia dieneri* Nakazawa (Feng *et al.*, 2007; He *et al.*, 2007). Although the index taxon for the PTB (*H. parvus*) has not been recovered at Dongpan, these fossils finds support placement of the PTB at the Bed 12/13 contact (Fig. 2; Yin *et al.*, 2007).

METHODS AND MATERIALS

Petrographic analyses

A total of 101 samples were collected and analyzed petrographically in this study. Radiolarians were extracted using the technique of Pessagno & Newport (1972). Samples were placed in dilute (3%) hydrofluoric acid for 8 h and then rinsed. After repetition of this process for 2 weeks, the residues were sieved (0.054 mm) and dried. About 9000 individual radiolarian tests representing four taxonomic orders were recovered from the Upper Permian of the Dongpan section. Taxonomic abundances were calculated from 50 fields of view; specimens were counted as whole fossils when the shell was at least three-quarters preserved. Specimens were recovered from the dry residue with a fine brush under a stereoscopic microscope for taxonomic identification. The best-preserved specimens were mounted on stubs and photographed with a scanning electronic microscope (SEM) for more precise determinations. Sample diversity was calculated on the basis of SEM analysis.

Fifty grams of each sample were processed using standard palynological methods (Albani *et al.*, 2006). The sample was spiked with a known number of lycopodium spores, and the mixture was then treated with hydrochloric acid (36.5%) and hydrofluoric acid (40%). The residue was sieved in pure ethanol and then concentrated using zinc bromide solution (S.G. 2.5). Neither oxidative nor alkali treatments were applied. Owing to its composition, charcoal is not chemically destroyed during the processing of sediment samples for fossil pollen analysis. We determined the concentrations of algae, spores and pollen, and charcoal fragments by measuring the frequency ratio of each of these components to lycopodium spores in the concentrated residues using light microscopy and scanning electron microscopy.

One of the major problems in petrographic quantification of microscopic charcoal is that of differentiating these particles from carbonized plant fragments. In the study samples, particles that were jet black, completely opaque, angular, and showed little or no cellular structure were categorized as charcoal; partially carbonized brown or incompletely opaque particles were not included. Charcoal particles varied in shape and size, ranging from <5 to >10 000 μm^2 . Care was taken

to distinguish other types of opaque particles in the pollen preparations, including pyrite, marcasite, and biotite, although totally unequivocal identification was not always possible.

Geochemical and mineralogic analyses

A total of 53 samples from Dongpan section were trimmed to remove visible veins and weathered surfaces and pulverized to ~200 mesh size in an agate mortar. Major element abundances were determined by wavelength-dispersive X-ray fluorescence (XRF) analysis on fused glass beads using a XRF-1800 at the Key Laboratory of Biogeology and Environmental Geology of the Ministry of Education, China University of Geosciences (Wuhan).

Trace elements and rare earth elements (REEs) were measured by Agilent 7500a inductively coupled plasma mass spectrometry (ICP-MS) at the State Key Laboratory of Geological Processes and Mineral Resources, China University of Geosciences (Wuhan). About 50 mg of each sample powder were weighed into a Teflon bomb and then moistened with a few drops of ultrapure water before addition of 1 mL HNO₃ and 1 mL HF. The sealed bomb was heated at 190°C in an oven for more than 48 h. After cooling, the bomb was opened and evaporated at 115°C to incipient dryness, then 1 mL HNO₃ was added and the sample was dried again. The resultant salt was re-dissolved with 3 mL 30% HNO₃ before it was again sealed and heated in the bomb at 190°C for 12 h. The final solution was transferred to a polyethylene bottle and diluted in 2% HNO₃ to about 80 mL for ICP-MS analysis. Analysis of the international rock standards BHVO-2 and BCR-2 indicated that the analytical precision is mostly better than 5%, according to the RSD.

Powdered samples were placed in aluminum holders and scanned by X-ray diffraction (XRD) using a D/max-3B at the State Key Laboratory of Geological Processes and Mineral Resources, China University of Geosciences (Wuhan). Samples were scanned from 2° to 32°2θ at 0.2° min⁻¹ using CuKα radiation and a graphite monochromator. For clay fraction analysis, a portion of each sample was suspended in distilled water after particle separation by ultrasonic disaggregation. The <2-μm size fraction was recovered by ultracentrifugation and air-dried prior to making oriented slides by standard smear techniques.

Geochemical concentration data were used to estimate the relative proportions of the major fractions of each sample as follows:

$$\text{Clay minerals (\%)} = \text{Al}_{\text{meas}} \times 100 / \kappa_1 \quad (1)$$

$$\text{Excess SiO}_2 (\%) = \text{SiO}_{2(\text{meas})} - (\text{Al}_{\text{meas}} / 27.0 \times \kappa_2 \times 60.1) \quad (2)$$

Equations 1 and 2 are formulas for calculating model amounts of clay minerals and excess SiO₂ (see Geochemical

proxies for productivity) in a sample based on measured Al and SiO₂ concentrations conforming to the dominant mineralogy of the sample, as determined by XRD analysis (cf. Algeo *et al.*, 2007b). The coefficients 27.0 and 60.1 represent the molar weights in grams of Al, and SiO₂, respectively, and the constants κ₁ and κ₂ represent the average concentration of Al and the average molar Si:Al ratio of the clay mineral assemblage, respectively. Values of 13.0 for κ₁ and 2.0 for κ₂ were found to minimize variance about a mean sum of 100% for the samples as a group.

Excess barium (Ba_{xs}) was calculated as:

$$\text{Ba}_{\text{xs}} = \text{Ba}_{\text{meas}} - \text{Al}_{\text{meas}} * 24.0 \quad (3)$$

where the constant 24.0 represents the inferred ratio of detrital Ba/Al (in units of ppm/% or 10⁻⁴) in the study section (see Geochemical proxies for productivity).

The chemical index of alteration (CIA) was calculated using weight fractions of major oxides as follows:

$$\text{CIA} = \text{Al}_2\text{O}_3 / (\text{Al}_2\text{O}_3 + \text{K}_2\text{O} + \text{Na}_2\text{O} + \text{CaO}_{\text{noncarb}}) \quad (4)$$

where CaO_{noncarb} represents the weight fraction of CaO present in non-carbonate phases, which was calculated as CaO_{total} - CaCO₃ × 56.1/100.1, where 56.1 and 100.1 are the molar weights in grams of CaO and CaCO₃.

Europium (Eu) and cerium (Ce) are the only REEs to have multiple valences, making them subject to fractionation that can be represented as Eu and Ce anomalies (de Baar *et al.*, 1985; German & Elderfield, 1990). These anomalies were calculated as follows:

$$\text{Eu}/\text{Eu}^* = 2 \times \text{Eu}_\text{N} / (\text{Sm}_\text{N} + \text{Gd}_\text{N}) \quad (5)$$

$$\text{Ce}/\text{Ce}^* = 2 \times \text{Ce}_\text{N} / (\text{La}_\text{N} + \text{Pr}_\text{N}) \quad (6)$$

where the subscript 'N' represents the Post-Archean Average Shale (PAAS)-normalized concentration of a given element (Taylor & McLennan, 1985; McLennan, 2001). Ce anomalies also can be calculated as 3 × Ce_N / (2 × La_N + Nd_N); for Dongpan, this equation yielded almost identical values to equation 6. La_N/Yb_N and Sm_N/Yb_N ratios were calculated as proxies for the relative enrichments of light to heavy REEs (LREE/HREE) and middle to heavy REEs (MREE/HREE), respectively (Correction added after publication 3 November 2011: Equations 5 and 6 and equation in preceding sentence was amended.). Although LREE/HREE ratios are sometimes calculated as La_N/Lu_N, Yb is preferred over Lu (e.g., Sholkovitz *et al.*, 1994; Lécuyer *et al.*, 2004) owing to the irregular odd/even abundance patterns among REEs (Elderfield, 1988). Sm is used to represent MREEs rather than Gd because the latter element may be subject to anomalies in seawater (de Baar *et al.*, 1985; Alibo & Nozaki, 1999).

C and S elemental concentrations were measured using an Eltra 2000 C-S analyzer at the University of Cincinnati. Data quality was monitored via multiple analyses of USGS SDO-1

standard, yielding an analytical precision (2σ) of $\pm 2.5\%$ of reported values for C and $\pm 5\%$ for S. An aliquot of each sample was digested in 2N HCl at 50°C for 6 h to dissolve carbonate minerals, and the residue was analyzed for total organic carbon (TOC) and non-acid-volatile sulfur (NAVS); total inorganic carbon (TIC) and acid-volatile sulfur (AVS) were obtained by difference.

The magnetic susceptibility (MS) of samples was measured using a high-sensitivity susceptibility bridge at Louisiana State University. The susceptibility bridge was calibrated using standard salts, for which values are given in Swartzendruber (1992) and the Handbook of Physics and Chemistry (2004). Reported MS values represent the mean of three measurements in units of $\text{m}^3 \text{kg}^{-1}$. MS is reported here in terms of sample mass, because it is easier and faster to measure with high precision than volumetric analyses (Ellwood *et al.*, 2008).

RESULTS

Petrographic analyses

Radiolarian systematics of the Dongpan section were previously reported by Feng *et al.* (2000), Feng & Gu (2002), and Feng *et al.* (2007); point-count results are given in Table 1. The order Albaillellaria exhibits a general increase in diversity and abundance from the base of the study section to a maximum around the Bed 4/5 contact, followed by a marked decline in diversity upsection to Bentonite 2 (Fig. 3A,B). The other three orders of radiolarians (Latentifistularia, Spumellaria, and Entactinaria) exhibit general increases in diversity and abundance upsection to Bentonite 2, apart from a short-term decline associated with Bentonite 1 (Fig. 3C–H). At the level of Bentonite 2, all radiolarian orders exhibit abrupt and drastic declines in diversity (-58% to -81%) and abundance (-85% to -88%), with the Albaillellaria going entirely extinct. The other three orders show a modest recovery in the lower part of Bed 7, followed by a second period of decline in the upper part of Bed 7 and Bed 8 during which many of the surviving species went extinct (the ‘extinction phase’ of Feng *et al.*, 2007). For each order, abundance and diversity covary positively throughout the study section.

The organic fraction of the study section consists of spores and pollen, algae and acritarchs, and charcoal fragments (Fig. 4); point-count results are given in Table 2. Diverse and abundant palynomorphs occur in the Upper Permian Dalong Formation, including approximately 17 species (12 genera) of spore and pollen, eight species (six genera: *Leiosphaeridia*, *Schizosporis*, *Verybachiium*, *Micrhystridium*, *Baltisphaeridium* and *Dictyotidium*) of acritarchs, one species of algal cyst (*Tymanicysta stoschiana*), and three kinds of unidentified tracheids (Fig. 4). On the other hand, assemblages from the Lower Triassic Luolou Formation lack diversity and consist mainly of acritarchs and a few miospores. The types of spore and pollen found at Dongpan are typical of latest Permian and

earliest Triassic sediments elsewhere in China. The percentage of pteridophyte spores is relatively low, whereas gymnosperm pollen is dominant throughout the Dongpan section. Whether the pollen and spore record is truly representative of the parent vegetation on adjacent landmasses is uncertain for a distal marine site such as Dongpan.

Acritarchs are small organic structures of varying origins, although one common type is the resting cysts of dinoflagellata or chlorophyta (green algae). At Dongpan, marine algal and acritarch concentrations are moderate below the level of Bentonite 1, except for two concentration spikes that are evident within Beds 2 and 3 (Fig. 5A). An increase in algal and acritarch abundance is observed within Bed 5, peaking about 25 cm below Bentonite 2, followed by a sharp decline to near-zero values in the upper part of Bed 5. Above Bentonite 2, low concentrations persist (except for a few samples) to the top of the study section.

The concentrations of spores and pollen derived from terrestrial higher plants are generally low through the lower part of the study section but increase slightly just below an ash layer in the middle of Bed 2 and again below Bentonite 1 (Fig. 5B). A large ($>20\times$ relative to background values), sharp increase in spore and pollen abundance is observed in the 15 cm below Bentonite 2. Concentrations fall again within Bentonite 2, but Beds 6–9 contain markedly greater amounts ($\sim 5\times$ background) of spores and pollen than those below the Bed 5 peak. In the overlying Beds 10–13, spore and pollen exhibit the low concentrations characteristic of the lower part of the section.

Charcoal particles are present in generally low to moderate concentrations below Bentonite 2 (Fig. 5C). Small peaks are evident below an ash layer in the middle of Bed 2 and below Bentonite 1 in the upper part of Bed 3, and these increases correlate with the larger increases in algal and acritarch concentrations observed at the same levels (Fig. 5A). A much larger spike in charcoal particle concentration commences below Bentonite 2 but peaks immediately above it, and this is followed by additional peaks within Beds 8–9, 11–, and 14 (Fig. 5C). Peak concentrations are $\sim 5\times$ to $10\times$ those of the background values in the lower part of the study section. Field observations at a finer stratigraphic scale suggest that charcoal particles may be concentrated toward the base and top of each bentonite.

Geochemical proxies for productivity

Total organic carbon (TOC) is low throughout the study section, with all samples yielding concentrations $<0.25\%$ (Fig. 5D). Total sulfur (TS) is low throughout the study section also, with all samples yielding concentrations $<0.04\%$. Neither TOC nor TS shows a definite stratigraphic trend within the section, nor is there any clear relationship to bentonites.

The excess SiO_2 present in the study section (calculated per equation 2) is inferred to represent biogenic silica of radiolar-

Table 1 Dongpan section radiolarian point-count data. Shen *et al.*, 'Volcanic perturbations of the marine environment in South China preceding the latest Permian mass extinction and their biotic effects'

Bed	Sample	Albaillellaria		Latentifistularia		Spumellaria		Entactinaria		Total	
		Diversity	Abundance	Diversity	Abundance	Diversity	Abundance	Diversity	Abundance	Diversity	Abundance
12	29	0	0	0	0	2	3	3	15	5	18
12	28	0	0	0	0	2	11	2	13	4	24
12	27	0	0	0	0	2	11	2	11	4	22
11	26	0	0	0	0	2	15	3	18	5	33
10	25	0	0	0	0	2	10	4	16	6	26
10	24	0	0	0	0	3	14	4	16	7	30
9	23	0	0	0	0	4	18	5	20	9	38
8	22	0	0	0	0	6	30	5	18	11	48
7	21	0	0	3	17	13	33	8	26	24	76
7	20	0	0	3	17	11	37	8	21	22	75
7	19	0	0	15	44	4	16	6	22	25	82
6	18	–	–	–	–	–	–	–	–	–	–
5	17	3	44	36	286	21	115	27	188	87	633
5	16	1	17	27	225	18	71	27	151	73	464
5	15	8	44	35	240	18	90	25	150	86	524
4	14	2	11	11	33	12	30	18	44	43	118
3	13	9	36	20	129	18	81	17	121	64	367
3	12	2	24	15	118	16	67	16	76	49	285
3	11	6	28	14	102	16	95	14	90	50	315
2	10	4	32	21	153	16	71	20	135	61	391
2	9	0	0	18	104	16	71	17	65	51	240
2	8	2	19	25	152	13	49	16	93	56	313
2	7	0	0	13	95	12	65	16	109	41	269
2	6	5	40	26	215	13	54	17	142	61	451
2	5	0	0	11	78	14	77	14	65	39	220
2	4	1	15	13	102	10	55	15	93	39	265
2	3	2	14	17	95	14	48	12	70	45	227
2	2	2	23	12	81	12	65	15	88	41	257
2	1	3	44	19	147	15	79	26	194	63	464

ian origin. Other potential sources of SiO₂ are unlikely: (i) field and petrographic observations revealed no quartz silt or siliceous sponges; (ii) excess SiO₂ concentrations within the bentonite samples are similar to or somewhat lower than values for other lithologies (Fig. 5E), making a volcanic ash source unlikely; and (iii) excess SiO₂ concentrations closely mirror radiolarian abundance patterns (Fig. 3), consistent with a radiolarian source. Below the LPME, biogenic SiO₂ concentrations range from 10% to 70%, averaging ~40% (Fig. 5E). No stratigraphic trend is apparent from the base of the section to the level of Bentonite 2, and bed-to-bed variation within this interval is considerable. The interval between Bentonite 2 and the LPME shows a steady decline in biogenic SiO₂ (from 65% to 30%), which is followed by a further abrupt decline (to 10%) in conjunction with the LPME. Biogenic SiO₂ concentrations exhibit a modest increase in the first meter above the LPME (to 25%) but then decline again in the uppermost part of the study section.

Excess Ba (Ba_{xs}) concentrations were calculated using an inferred detrital Ba/Al ratio of 24.0 based on fitting a line to the samples showing the lowest Ba concentrations (Fig. 6A). Total Ba exhibits significant negative covariation with Al, indicating that Ba_{xs} is a valid paleoceanographic proxy and not simply an artifact of the calculation procedure. Ba_{xs} ranges

from 0 to 1600 ppm below the LPME (averaging ~300 ppm), with local spikes within Bed 2 and (less strongly) Bed 7 (Fig. 5F). Low values (<100 ppm) are associated with Bentonites 1 and 2, and Ba_{xs} concentrations decrease to nearly zero at the LPME horizon. Although the biogenic SiO₂ profile (Fig. 5E) exhibits greater variance than Ba_{xs}, these two proxies exhibit statistically significant positive covariation (Fig. 6B), supporting their mutual use as paleoproductivity proxies. In addition, both productivity proxies exhibit statistically significant negative covariation with CIA, a weathering proxy (Fig. 6C–D).

Other geochemical and mineralogic proxies

X-ray diffraction results for major mineral and clay mineral fractions are given in Table 3, and elemental concentration data for major, trace, volatile, and REEs are given in Table 4. The main mineral phases in the study section are clays (20–85%) and biogenic silica (15–60%; Fig. 7A). Clay minerals average 50% and show considerable bed-to-bed variation below the LPME but increase to ~70% and show little bed-to-bed variation above the LPME. Being the second most abundant phase, biogenic SiO₂ varies in a complementary manner to clays. The alternation of clay-rich and SiO₂-rich

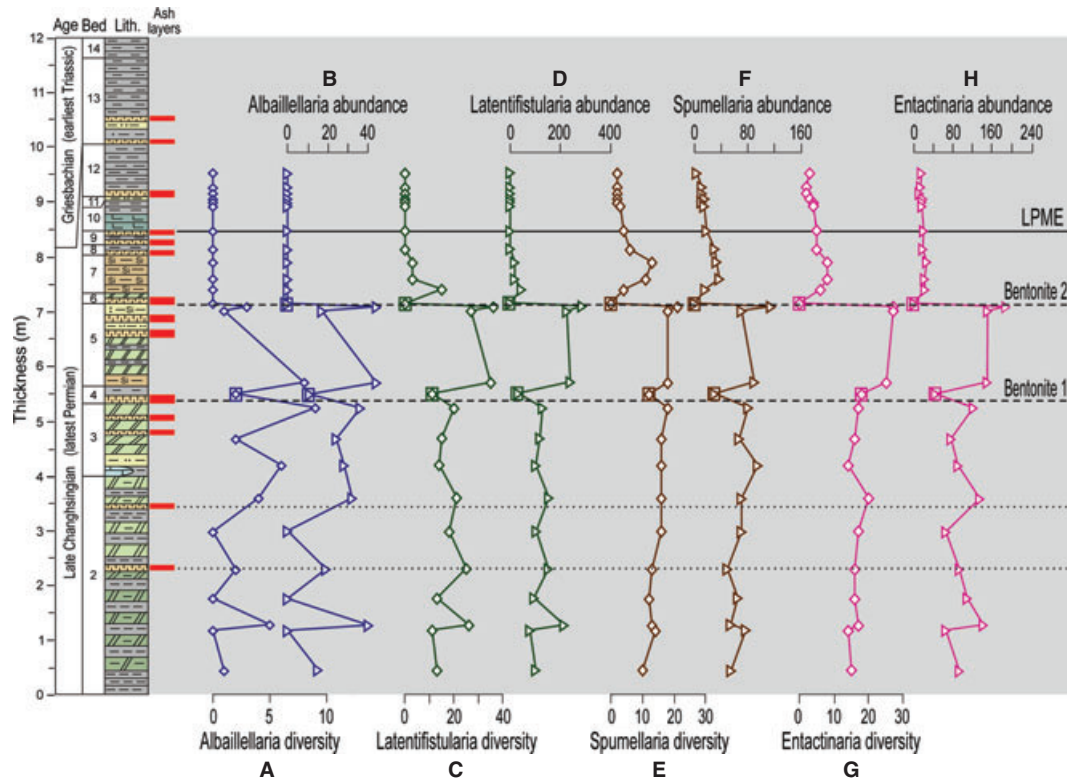


Fig. 3 Radiolarian diversity and abundance profiles for *Albaillellaria* (A,B), *Latentifistularia* (C,D), *Spumellaria* (E,F), and *Entactinaria* (G,H). Diversity and abundance data were calculated based on 50 microscopic fields of view. The horizontal lines represent the latest Permian mass extinction horizon (LPME; solid), Bentonites 1 and 2 (dashed), and thinner bentonites lower in the section (dotted). The stratigraphic position of ash layers in the section is shown by red bars in the 'ash layers' column; bentonite samples analyzed in this study are enclosed by squares. See Fig. 2 for lithologic key; lith. = lithologic column. See the studies by Feng *et al.* (2007) and He *et al.* (2007) for related paleobiological datasets.

layers reflects the gross lithology of the study section as described in the field (see Geological Setting and Stratigraphy). Other mineral fractions (e.g., calcite) are present in only limited quantities throughout the study section.

The clay fraction consists mainly of illite and smectite with subordinate amounts of mixed-layer I/S and kaolinite (Fig. 7B). The relative abundances of these clay minerals vary stratigraphically. Kaolinite is moderately abundant below the LPME, averaging 20% of the clay fraction, but this mineral disappears almost completely above the LPME. Smectite is abundant throughout the study section, peaking in abundance at 50–60% of the clay fraction; it covaries strongly with kaolinite where the latter mineral is present (i.e., below the LPME). Illite and mixed-layer I/S range in abundance from 15% to 100%, and these clays tend to be dominant in stratigraphic intervals characterized by high total clay abundance (Fig. 7A). Illite increasingly dominates the clay mineral fraction above the LPME.

The chemical index of alteration (CIA) is a commonly used proxy for the degree of weathering of siliciclastic sediments, with high values signifying more intense weathering (Price & Velbel, 2003). The ratio generally reflects the extent of con-

version of feldspars to clay minerals, especially cation-poor clays such as kaolinite (Sutton & Maynard, 1993). At Dongpan, CIA values range from 0.73 to 0.88 but most (95%) of the section yields values between 0.78 and 0.82 (Fig. 7C). Values outside this range are distributed sporadically, with a minimum (0.73) in the upper part of Bed 2, a maximum (0.88) at the level of Bentonite 1, and a local peak (0.82) at the level of Bentonite 2. The LPME is associated with a small but well-defined excursion toward higher CIA values (from 0.77 to 0.80).

Magnetic susceptibility (MS) is a measure of the magnetism acquired by a sample in a low-strength inducing magnetic field. It is largely a function of the concentration of magnetizable minerals in a sample, including ferrimagnetic and antiferromagnetic phases (e.g., Fe oxides and Fe sulfides), less strongly magnetic or 'paramagnetic' phases (e.g., clay minerals such as illite, smectite, and chlorite), and negatively magnetic or 'diamagnetic' phases (e.g., calcite, quartz, and organic matter) that reduce total sample MS (Ellwood *et al.*, 2000). In siliciclastic sections, MS is often a useful proxy for grain size, with higher values indicative of higher clay content (Ellwood *et al.*, 2008, 2011). At Dongpan, MS values are

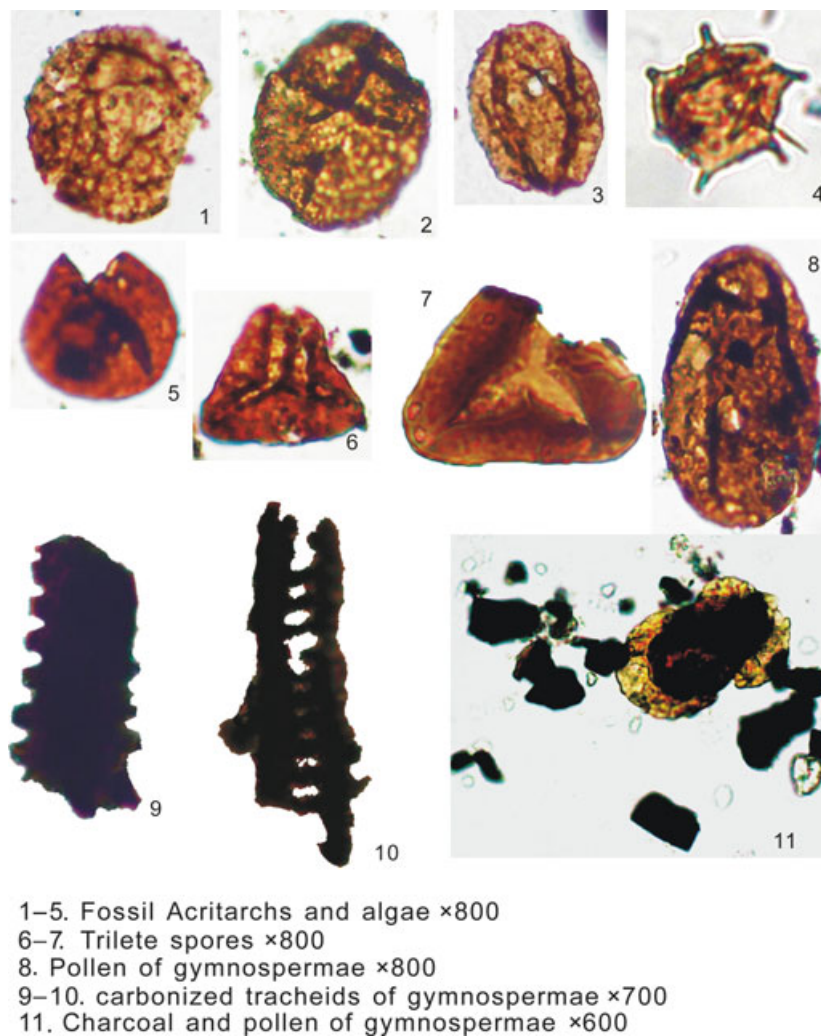


Fig. 4 Photomicrographs of acritarchs and algae (1–5), spores and pollen (6–8), carbonized tracheids (9–10), and charcoal (11).

mostly between 0.3 and $0.8 \times 10^{-7} \text{ m}^3 \text{ kg}^{-1}$ (Fig. 6D). Transient increases are observed at the levels of Bentonite 2 and especially the LPME, the latter yielding a maximum of $2.05 \times 10^{-7} \text{ m}^3 \text{ kg}^{-1}$. Average MS values are higher above the LPME ($\sim 0.6 \text{ m}^3 \text{ kg}^{-1}$) than below it ($\sim 0.4 \text{ m}^3 \text{ kg}^{-1}$).

The section contains only insignificant amounts of pyrite, as shown by uniformly low total S concentrations ($<0.04\%$; Fig. 6E). Fe_T/Al ratios average 0.39 ± 0.12 (Fig. 6F), which is slightly lower than the average of 0.50 for upper continental crust (Lyons & Severmann, 2006). Most excursions to Fe_T/Al ratios >0.50 are represented by single samples and, hence, of uncertain significance; only the excursion in the middle of Bed 7 yielding the peak Fe_T/Al ratio (0.70) is represented by multiple samples.

Redox-sensitive trace-metal concentrations at Dongpan are mostly close to those found in typical organic-lean shales. For example, the aluminum-normalized ratios of vanadium (V/Al) and uranium (U/Al) average 12×10^{-4} and 0.40×10^{-4} , respectively, equal to or lower than values of

18×10^{-4} and 0.40×10^{-4} for PAAS (Figs. 7G,H; Taylor & McLennan, 1985; McLennan, 2001). Although charcoal can potentially adsorb large amounts of trace metals from seawater, especially when possessing a high ion-adsorptive capacity in its 'activated' state (Brown & Parks, 2002), the Dongpan section shows no apparent relationship between trace-metal concentrations (Fig. 7) and charcoal (Fig. 5). However, substantial changes in trace-metal concentrations are associated with Bentonites 1 and 2, where V/Al exhibits minimum values and U/Al maximum values; smaller changes of the same sign are evident within Bed 2 (dotted horizontal lines; Fig. 7). Both metals show only minor concentration changes at the LPME horizon.

REE geochemistry

Eu does not fractionate readily at Earth-surface temperatures, so Eu anomalies (Eu/Eu^*) in sediments are generally inherited from source materials (Elderfield, 1988). Ratios between

Table 2 Dongpan section organic fraction point-count data. Shen *et al.*, 'Volcanic perturbations of the marine environment in South China preceding the latest Permian mass extinction and their biotic effects'

Sample	Depth (cm)	Spores and pollen (normalized)	Algae and acritarchs (normalized)	Charcoal fragments (normalized)
13-9	1150	0	0	8
13-8	1125	0	0	7
13-7	1005	0	0	0.3
13-6	1075	0	0	1
13-5	1050	0.4	0	2.4
13-4	1025	0.3	0.3	0.4
13-3	1002.5	0	0	4
13-2	1002	0	0	0.2
13-1	1001	0.3	0.4	0.6
12-3-4	950	0	0	1.4
12-3-3	942	0	0	1.6
12-3-2	934	0	0	0.6
12-3-1	924	0.5	0	7.5
12-1-3	918	0.7	0	5.7
12-1-2	912.5	0.7	0	2.3
12-1-1	908	1	0	0.8
11	902.5	0.3	0	1.6
10-3	896.5	0.7	0	8.3
9-5	840	0	0	2
9-4	823.5	0	0	11.5
9-3	820	0	0	7
9-2	817	1	0	5.7
9-1-2	815	0	0	0.3
9-1-1	813	0	0.6	0
8-7	810.5	0	0	9.5
8-6	809	0	0.5	8
8-5	807	0.3	0.7	4.3
8-4	805	0	0	2.3
8-3	803	0	0.2	0.3
8-2	802	0.5	0	0.5
8-1	801	1	0.5	3
7-8-2	795	1	0	4.5
7-8-1	792	2	0.7	1.3
7-7	787	0.5	0	0.7
7-6	767	1	0	2
7-5	757	1.8	0.8	3.2
7-4-2	754	1.8	0.8	3.2
7-4-1	749	0.7	0	2.5
7-3	747	0.2	0	0.8
7-2	742	0	0	0.1
7-1	737	0.6	0.1	1.2
6-4	732	0	0	0.3
6-3	727	0	0	0.1
6-2	720	0	0	0.5
5-19-2	714	0.2	0.1	0.7
5-19-1	706	0.5	0	1.4
5-18	703	0	0.1	0.1
5-17	698	2	0.3	5.7
5-16-2	691	1	0.1	0.8
5-16-1	683	8	1.8	1
5-14	677	9.3	1	2.3
5-13	669	0	0	0
5-12	662	0	0.8	3
5-11	656	0	1	2.3
5-10	649	0.1	0.3	1.6
5-8-5	632	0	1.5	1.3
5-8-1	625	0	0.8	0.3

Table 2 (Continued)

Sample	Depth (cm)	Spores and pollen (normalized)	Algae and acritarchs (normalized)	Charcoal fragments (normalized)
5-6-5	617	0.2	0.2	1.2
5-6-1	609	0.1	0.3	1.6
5-4-1	601	0	0.4	0.3
5-3-2	592	0	0.8	0.3
5-2	571	0	0.5	0.5
5-1	568	0	0.1	0.6
3-1-2	530	0.3	0.5	0.7
3-1-3	524	0.2	0.2	0.9
3-3	512	0	0.6	1.4
3-5	497.5	1	5	1
3-7	482	0.5	2.5	1
3-9	474	0.5	0.3	2
3-11	468.5	0.5	1	3.5
3-13-1	445	0.5	0.3	1.5
3-13-3	439	0.1	0.3	0
3-14	434.5	0.3	0.3	0.6
3-15-2	427	0	0.2	0.5
3-16	419.5	0	0.2	0.5
3-17	404.5	0	0.1	0.6
2-2-1	362	0.5	0.1	0.1
2-2-3	359.5	0	0	0
2-4	373	0.2	0.2	0
2-6	299	0	0.3	1.3
2-8	282	0	0.5	1
2-10-1	258	0.4	0	0.4
2-10-3	254	0.3	0.3	0
2-10-5	250.5	0	0	0
2-10-7	246	0.6	0.1	0
2-10-9	242	1	0.5	0
2-12	230	0	0	0.6
2-13-2	214	0	0.2	0
2-14	206	0.1	0.3	0.1
2-15-2	192	0	0.2	0
2-16-1	173	0.2	0.1	0
2-16-3	176.5	1	4	2
2-18-6	132	0.5	0.3	2
2-18-8	128.5	1	0	4
2-19	118.5	0.2	0.1	1
2-20-4	85.5	0.3	0.2	1.3
2-21	62	0.2	0.2	1.2
2-23	45.5	0.1	0.4	2.2
2-27	0	0	0.4	2.2
2-29	-30	0.1	0.2	0.6
2-31	-60	0.3	0.5	1.5

LREEs, MREEs, and HREEs are also commonly used to characterize detrital and hydrogenous sources of REEs (e.g., Musashino, 1990; Lécuyer *et al.*, 2004) as well as interelemental fractionation processes (e.g., Sholkovitz, 1992; Sholkovitz *et al.*, 1994, 1999). REE profiles show a strong relationship to bentonites at Dongpan. Eu anomalies (Eu/Eu^*) vary between 0.7 and 1.0 through most of the section but decrease to 0.37–0.40 within Bentonites 1 and 2 (Fig. 8A). Modest excursions to lower Eu/Eu^* values are seen also at several levels within Bed 2 (dotted horizontal lines; Fig. 8). La_N/Yb_N and Sm_N/Yb_N ratios vary mostly in the

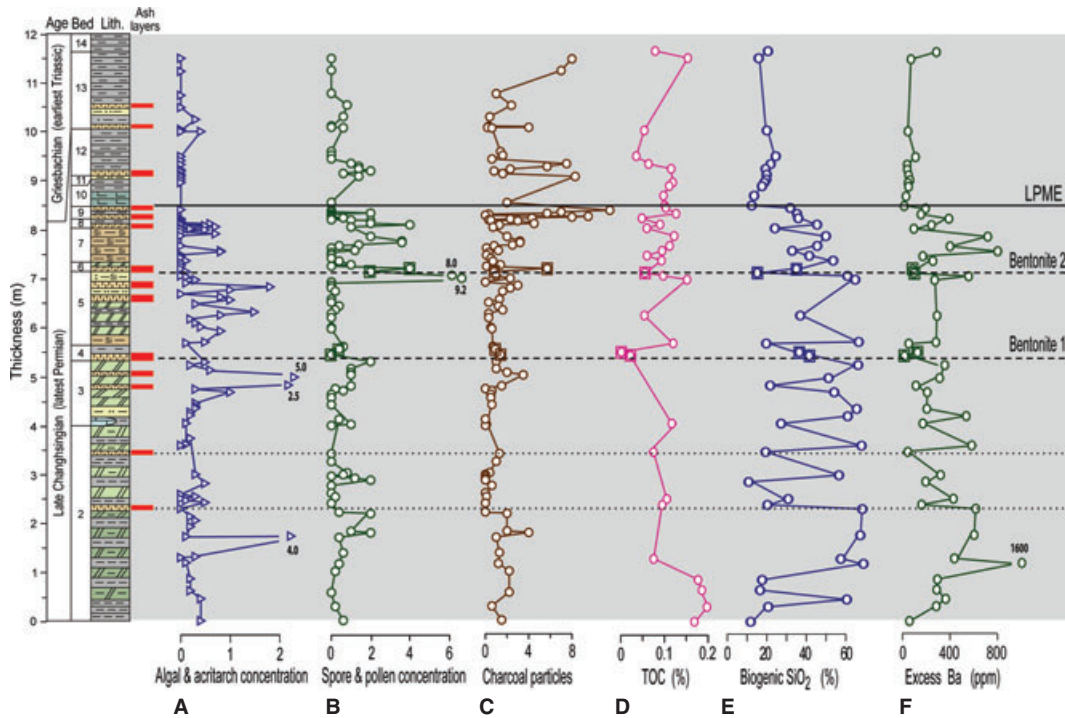


Fig. 5 Bio/chemostratigraphic data: (A) Algal and acritarch abundance; (B) Spore and pollen abundance; (C) Charcoal particle abundance; (D) Total organic carbon (TOC); (E) Biogenic SiO_2 , calculated per equation 2; and (F) Excess Ba, calculated per equation 3. Bentonite samples analyzed in this study are enclosed by squares. Other features as in Fig. 3.

range of 1.0–1.8, but La_N/Yb_N decreases to 0.45–0.60 and Sm_N/Yb_N to 0.6–0.7 within Bentonites 1 and 2 (Fig. 8B,C). These proxies document the strong HREE enrichment of the bentonites that is apparent in a standard REE distribution (Fig. 9, inset). A crossplot of Eu/Eu^* vs. La_N/Yb_N shows that the bentonites can be clearly separated from other lithologies on the basis of REE chemistry (Fig. 9). For the non-bentonitic samples, there is a small change in average REE composition across the LPME although substantial overlap exists.

Ce anomalies are a useful paleoredox proxy (German & Elderfield, 1990; Kakuwa & Matsumoto, 2006). Under oxidizing conditions, Ce^{+4} is separated from other REEs in seawater (which exist only in the +3 valence, except for Eu), yielding a Ce/Ce^* ratio of 0.2–0.6 for modern seawater (Sholkovitz *et al.*, 1994). Under reducing conditions, Ce^{+3} is not fractionated relative to other REEs, yielding a Ce/Ce^* ratio close to 1.0. At Dongpan, Ce anomalies (Ce/Ce^*) range from 0.43 to 1.08 (average = 0.80; Fig. 8D). The lower part of the study section (below Bentonite 1) shows substantial bed-to-bed variation of uncertain significance. Higher in the section, variation in Ce anomalies is closely related to event horizons: Ce/Ce^* values shift abruptly to higher values in conjunction with Bentonite 1 (from 0.45 to 1.05), Bentonite 2 (0.55–0.95), and the LPME (0.70–0.95). In each case, the high ratios are sustained for some distance (~ 0.5 m) upsection of the event horizon, indicating that the shifts in Ce/Ce^*

ratios are not controlled by sediment provenance (as for the other REE proxies above) but, rather, by environmental factors (see Marine redox conditions). Between event horizons, there is generally an irregular upsection trend toward lower Ce/Ce^* values (see Beds 5 or 7–9, for example).

DISCUSSION

Volcanic episodes

Bentonites 1 and 2 are whitish-gray claystones, respectively ~ 35 and ~ 25 cm thick, that contain large quantities of bipyramidal quartz, apatite, and zircon phenocrysts (Meng *et al.*, 2005; cf. Yin *et al.*, 1992). Volcanic ash layers are sometimes distinguished as ‘bentonites’ vs. ‘tonsteins’ depending on the relative proportions of smectite and kaolinite (Chamley, 1989). Formation of smectite typically involves uptake of Mg from seawater or porewater under neutral to alkaline conditions, whereas formation of kaolinite is favored by acidic conditions that result in strong cation leaching, as in association with coals in terrestrial environments (Staub & Cohen, 1978; Maliva *et al.*, 1999). At Dongpan, Bentonites 1 and 2 contain elevated concentrations of both smectite and kaolinite relative to background shales, in which the clay mineral assemblage is dominantly illitic (Fig. 7B). If kaolinite represents an in-situ alteration product, its abundance is unusual in view of deposi-

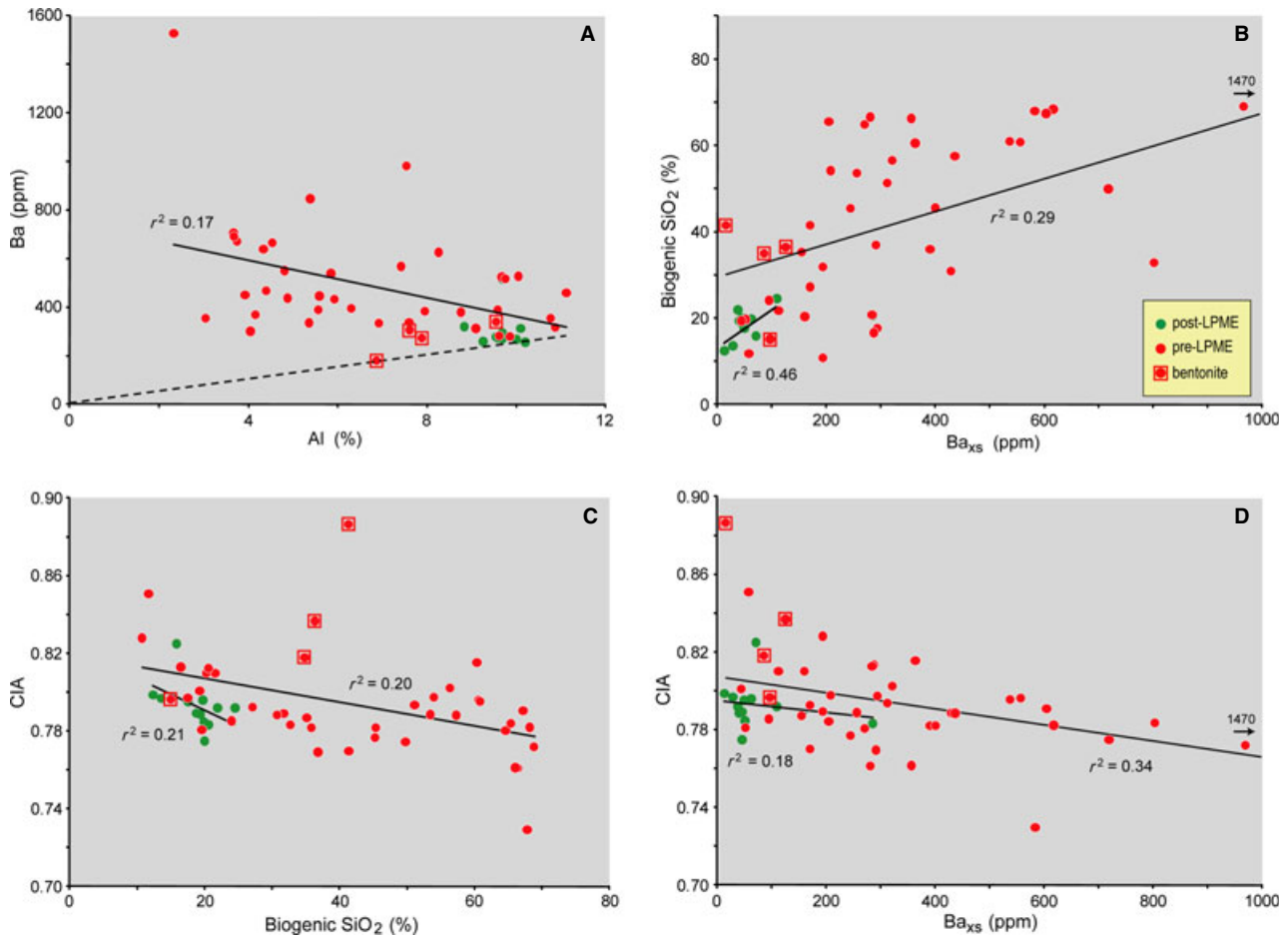


Fig. 6 Productivity proxies (biogenic SiO_2 , Ba_{XS}) and their relationships to chemical index of alteration (CIA): (A) Ba vs. Al. (B) Biogenic SiO_2 vs. Ba_{XS} . (C) Biogenic SiO_2 vs. CIA. (D) Ba_{XS} vs. CIA. In A, the dashed line represents the inferred detrital Ba/Al ratio of 24.0, and the difference between this line and a given sample point represents the amount of excess Ba. Red and green data points represent pre-LPME and post-LPME samples, respectively; bentonite samples analyzed in this study are enclosed by squares. All correlation coefficients (r^2) shown are significant at $p(\alpha) < 0.01$. Other features as in Fig. 3.

tion of Dongpan bentonites in a marine environment with low organic carbon concentrations and probably non-acidic porewaters (Fig. 5D). More likely is that kaolinite is a product of weathering of volcanic ashes in a subaerial setting followed by transport to the marine environment (e.g., Millot, 1970). This interpretation is supported by the fact that there is evidence of a volcanic component throughout the claystone beds of the Dongpan section (Meng *et al.*, 2005) and in other sections regionally (Yin *et al.*, 1992).

Bentonites 1 and 2 exhibit a highly distinctive REE chemistry, characterized by low Eu/Eu^* , $\text{La}_\text{N}/\text{Yb}_\text{N}$, and $\text{Sm}_\text{N}/\text{Yb}_\text{N}$ ratios (Figs 8 and 9). Low Eu/Eu^* values ($\sim < 0.5$) are typical of highly fractionated magmas, where Eu has been removed in early-crystallized phases (such as feldspars; e.g., Zhou *et al.*, 2005), leaving the residuum Eu-depleted (e.g., Zhong *et al.*, 2007). On the other hand, Eu/Eu^* values of 0.7–1.0 are typical of the upper continental crust and of clay minerals produced by crustal weathering (Taylor & McLennan, 1985; McLennan, 2001). The REE chemistry of bentonites at

Dongpan is similar to those at Xinmin, a deepwater PTB section in northern Guangxi Province (Fig. 1A) that contains at least 10 ash layers (Shen *et al.*, in review). Based on these two sample sets, we infer that the volcanic endmember has a Eu anomaly of < 0.60 and a $\text{La}_\text{N}/\text{Yb}_\text{N}$ ratio of < 1.0 (Fig. 9). Samples from below the LPME that show intermediate REE characteristics may contain a component of both volcanic ash and detrital material. However, there is no evidence of a volcanic fraction in the sediment above the LPME, where Eu/Eu^* and other REE proxies yield high and nearly uniform values (Figs 8 and 9).

The record of volcanic activity at Dongpan is not confined to Bentonites 1 and 2. Rather, the section contains dozens of thin (< 1 cm) as well as some thicker (1–10 cm) ash layers that were not sampled for this study. The stratigraphic distribution of these ash layers suggests temporally discrete episodes of volcanic activity during the latest Permian that we will refer to as ‘volcanic cycles’ (n.b., use of this term does not connote any extrinsic forcing or temporal regularity). Low-intensity pre-

Table 3 Dongpan section mineralogic and clay fraction XRD data. Shen *et al.*, 'Volcanic perturbations of the marine environment in South China preceding the latest Permian mass extinction and their biotic effects'

Sample	Elev (cm)	Total mineral				Clay mineral			
		Quartz (%)	Feldspar (%)	Calcite (%)	Clays (%)	Smectite (%)	Illite (%)	Kaolinite (%)	Mixed I/S (%)
DP-14-3	1174	30	15	0	55	55	45	0	0
DP-14-2	1164.5	30	10	0	60	0	100	0	0
DP-14-1	1154.5	30	15	0	55	64	36	0	0
DP-13-9-2	1150	35	10	0	55	55	45	0	0
DP-13-9-1	1094.5	35	15	0	50	60	40	0	0
DP-13-8	1087.5	20	10	0	70	50	50	0	0
DP-13-7	1051.5	35	10	0	55	45	55	0	0
DP-13-6	1039.5	50	5	0	45	0	100	0	0
DP-13-5	1011.5	40	10	0	50	0	100	0	0
DP-13-4	1010.5	40	10	0	50	20	80	0	0
DP-13-3	1002.5	40	5	0	55	0	100	0	0
DP-13-2	997.5	40	5	0	55	18	82	0	0
DP-13-1	979	5	0	0	95	21	0	0	79
DP-12-3-5	964	30	10	0	60	58	42	0	0
DP-12-3-4	950	25	10	0	65	46	54	0	0
DP-12-3-3	944	35	15	0	50	60	40	0	0
DP-12-3-2	934	10	5	0	85	0	35	0	65
DP-12-3-1	924	35	10	0	55	55	45	0	0
DP-12-1	912.5	40	5	0	55	55	45	0	0
DP-11	902.5	35	10	0	55	64	36	0	0
DP-10-3-3	890.5	35	10	0	55	64	36	0	0
DP-10-3-1	890.5	30	10	0	60	58	42	0	0
DP-10-1-9	885	35	5	0	60	58	42	0	0
DP-10-1-7	879.5	30	5	0	65	62	31	8	0
DP-10-1-5	869.5	25	5	0	70	64	36	0	0
DP-10-1-3	859.5	25	5	0	70	64	36	0	0
DP-10-1-1	849.5	25	5	0	70	43	36	21	0
DP-9-8	844.5	10	0	0	90	0	28	22	50
DP-9-7	836.5	15	0	0	85	0	24	24	53
DP-9-6	832.5	35	0	0	65	38	31	31	0
DP-9-4	823.5	30	5	0	65	31	31	0	38
DP-9-2	817.5	40	5	0	55	36	55	9	0
DP-8-7	810.5	40	0	0	60	33	50	17	0
DP-8-6	809	25	5	0	70	57	14	29	0
DP-8-5	806.5	35	5	0	60	42	33	25	0
DP-8-4	804	20	5	0	75	60	13	27	0
DP-8-3	803	30	5	0	65	38	46	15	0
DP-8-1	797	40	5	0	55	36	36	27	0
DP-7-7	787	45	5	0	50	40	40	20	0
DP-7-4	757	45	5	0	50	40	40	20	0
DP-7-1	737	55	5	0	40	25	50	25	0
DP-6-4	732	35	5	0	60	17	17	33	33
DP-6-3	724	55	5	0	40	25	25	25	25
DP-6-2	718	35	0	0	65	46	0	15	38
DP-6-1	712	30	0	0	70	43	0	0	57
DP-5-17	698	65	0	0	35	0	71	29	0
DP-5-16	695	35	0	0	65	0	31	23	46
DP-5-14	683	50	0	0	50	0	0	50	50
DP-5-12	675	40	5	0	55	0	45	0	55
DP-5-10B	654	45	0	0	55	18	55	27	0
DP-5-8	625	40	0	0	60	0	42	17	42
DP-5-6	603	35	5	0	60	0	33	17	50
DP-5-4	593	70	0	0	30	33	67	0	0
DP-5-1	568	55	5	0	40	25	38	38	0
DP-4-1	550	50	15	0	35	71	29	0	0
DP-4-2	543	50	0	0	50	50	10	40	0
DP-4-3	541	40	5	0	55	45	18	36	0

Table 3 (Continued)

Sample	Elev (cm)	Total mineral				Clay mineral			
		Quartz (%)	Feldspar (%)	Calcite (%)	Clays (%)	Smectite (%)	Illite (%)	Kaolinite (%)	Mixed I/S (%)
DP-3-1	524	45	5	0	50	20	40	0	40
DP-3-2	520	35	5	0	60	50	33	17	0
DP-3-3	510	50	5	0	45	56	33	11	0
DP-3-4	506	30	5	0	65	31	0	31	38
DP-3-5	497.5	40	5	0	55	45	36	0	18
DP-3-7	484	60	10	10	20	0	100	0	0
DP-3-8	482	30	5	0	65	46	31	0	23
DP-3-9	475.5	45	5	0	50	40	40	20	0
DP-3-11	468.5	40	0	0	60	33	33	17	17
DP-3-13	441.5	55	5	0	40	25	25	0	50
DP-3-14	434.5	55	5	0	40	50	50	0	0
DP-3-16	419.5	50	0	0	50	40	30	0	30
DP-3-17	404.5	45	15	0	40	88	13	0	0
DP-2-2	359.5	55	5	0	40	63	38	0	0
DP-2-3	346.5	15	5	0	80	25	0	6	69
DP-2-4	329.5	55	5	0	40	0	50	0	50
DP-2-5	316.5	10	5	5	80	25	0	6	69
DP-2-6	299	55	5	0	40	0	50	0	50
DP-2-9	286.5	45	5	0	50	20	30	0	50
DP-2-10	250.5	45	0	0	55	55	45	0	0
DP-2-11	238.5	30	0	0	70	71	14	14	0
DP-2-17	156.5	10	0	0	90	33	0	0	67
DP-2-18-1	128.5	50	0	0	50	40	20	0	40
DP-2-19	118.5	50	0	5	45	0	44	0	56
DP-2-20-2	90.5	55	0	5	40	0	50	25	25
DP-2-21	75.5	20	5	0	75	27	27	13	33
DP-2-22	64.5	35	0	0	65	54	23	23	0
DP-2-23	45.5	50	0	0	50	50	30	20	0
DP-2-24	30.5	30	0	0	70	29	29	0	43
DP-2-25	15	45	5	0	50	20	40	20	20
DP-2-26	0	35	5	0	60	25	0	0	75

cursor eruptions are indicated by a series of thin ash layers (see 'ash layers' column in Fig. 3) in the 40–60 cm immediately beneath the major ashfall layers, culminating in the major eruptions recorded by Bentonites 1 and 2. The inference of cyclic volcanic activity is also supported by a shift toward lower Eu/Eu* ratios within the same intervals (Fig. 8A). Beds 8 through 12, the ~2-m-thick interval bracketing the LPME, contain dozens of thin ash layers and thus are particularly rich in volcanic material (Meng *et al.*, 2005; Feng *et al.*, 2007) although the LPME itself is not associated with a bentonite.

Terrestrial vegetation and wildfires

Palynological data can provide information about conditions in land areas surrounding the Nanpanjiang Basin, including changes in vegetation, climate, and wildfires. For example, changes in the density of terrestrial floral cover and general condition of terrestrial ecosystems can be inferred from spore and pollen data. Increases in spore and pollen abundance immediately below the mid-Bed 2 ash layer and Bentonites 1 and 2 (Fig. 5B) suggest enhanced growth of conifer forests (i.e., the dominant sources of pollen) and/or increased stress

in terrestrial ecosystems in response to volcanic episodes. Possibly, conifers were favored over other types of terrestrial vegetation during the intervals of intensifying volcanic activity. The large increase in spore and pollen abundance between Bentonite 2 and the LPME may be an indication of a marked rise in stress in terrestrial ecosystems, triggering spore and pollen production (cf. Visscher *et al.*, 1996).

Changes in wildfire frequency can be inferred from secular variations in the abundance of charcoal particles. Combustion of plant material at temperatures of between 280 and 500°C yields a carbon residue that is typically black, opaque, and angular in form (Scott, 1989) and that is generally distinct from organic particles affected by bacterial decay (Guo & Bustin, 1998). At Dongpan, the abundance of charcoal particles generally rises with increasing volcanic activity, reaching peaks just below the mid-Bed 2 ash layer and Bentonites 1 and 2 (Fig. 5C). This observation implies more frequent wildfires during volcanic episodes, possibly a reflection of concurrent shifts toward conifer-dominated vegetation or of increased terrestrial ecosystem stress. However, other interpretations are possible, for example, volcanic eruptions resulted in widespread forest die-off, leaving dead timber that provided fuel

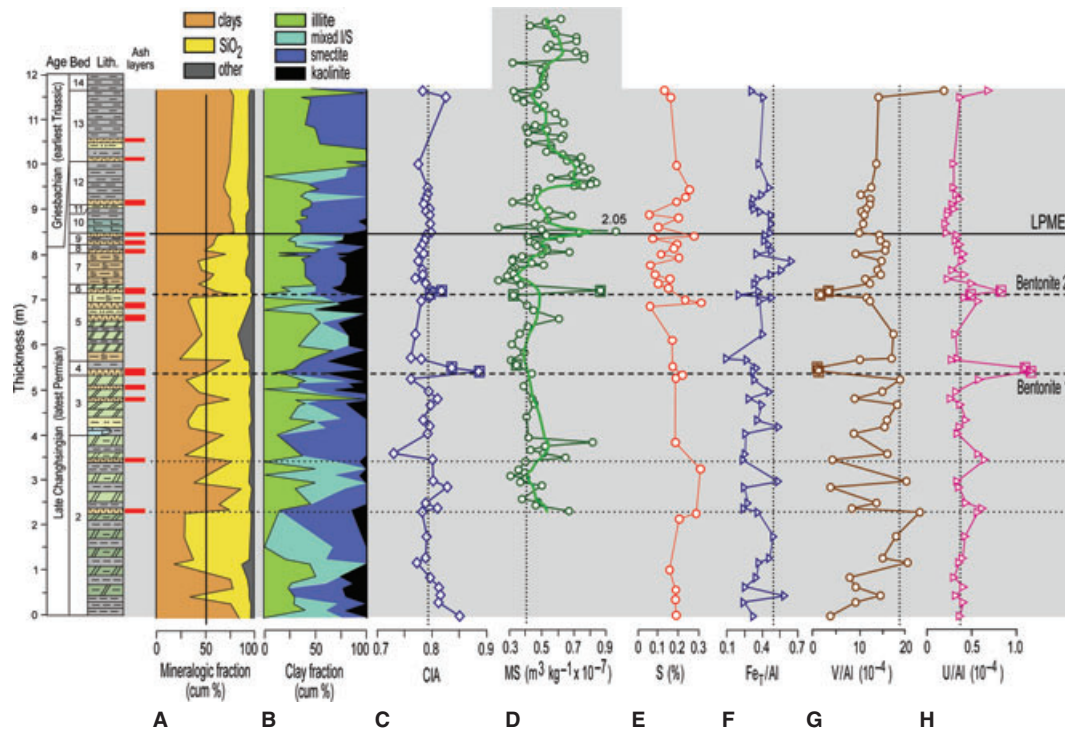


Fig. 7 Chemostratigraphic data: (A) Mineral fractions, calculated per equations 1 and 2. (B) Clay fractions, determined by XRF. (C) Chemical index of alteration (CIA), calculated per equation 4. (D) Magnetic susceptibility (MS). (E) S. (F) Fe_7/Al . (G) V/Al . (H) U/Al . MS was measured on a second sample suite with a stratigraphic range differing somewhat from the sample suite used for other analyses in this study. Bentonites samples analyzed in this study are enclosed by squares. Dotted vertical lines in C and D represent study-section averages and in F-H represent average crustal values (PAAS; Taylor & McLennan, 1985; McLennan, 2001). In G and H, units are 10^{-4} (i.e., ppm/%). Other features as in Fig. 3.

event horizons (i.e., Bentonites 1 and 2 and the LPME) yield ratios of 0.8–1.1, implying the development of anoxic conditions in conjunction with these events (Fig. 8D; n.b., high Ce/Ce^* ratios are found lower in the section also). Because the Fe-S and trace-metal proxies provide no evidence of a reducing benthic environment, we infer that the high Ce/Ce^* ratios represent the development or intensification of anoxia higher in the water column of the Nanpanjiang Basin. This interpretation is consistent with evidence of reduced levels of phytoplankton and zooplankton productivity at Dongpan in conjunction with the main event horizons (see Marine productivity), which may have declined in response to expansion of a regional OMZ (cf. Algeo *et al.*, 2007a). However, the possibility of lateral advection of the Ce/Ce^* redox signal over some greater distance (e.g., from the Tethyan Ocean) cannot be discounted based on existing data.

Expansion of a regional OMZ within the Nanpanjiang Basin is consistent with recent interpretations of general redox patterns in the Late Permian global ocean. The concept of whole-ocean ‘superanoxia’ (Isozaki, 1997) has been challenged on the basis of models documenting the difficulty of generating persistent deep-ocean anoxia (Kiehl & Shields, 2005; Winguth & Maier-Reimer, 2005) and geochemical evidence documenting redox changes primarily within the OMZ rather than in the deep ocean, which was probably mostly sub-

oxic during the latest Permian to Early Triassic (Algeo *et al.*, 2010, 2011a). In contrast, anoxia developed or intensified widely in intermediate-depth settings during the pre-LPME Changhsingian, as indicated by evidence from Meishan (Grice *et al.*, 2005; Cao *et al.*, 2009), Greenland (Nielsen & Shen, 2004), and western/northern North America (Wignall & Newton, 2003; Grasby & Beauchamp, 2009). Redox changes did not affect shallow-marine environments until the LPME; however, when oxic ocean-surface conditions began to be punctuated by recurrent brief episodes of anoxia (Algeo *et al.*, 2007a, 2008). Intermediate-depth settings probably experienced a further intensification of anoxia at this time (Brennecka *et al.*, 2011), setting the stage for episodic chemocline-upward excursions into the ocean-surface layer (Kump *et al.*, 2005).

Marine productivity

The LPME is widely characterized by major changes in phytoplankton assemblages and marine primary productivity rates (Grice *et al.*, 2005; Xie *et al.*, 2005; Payne & van de Schootbrugge, 2007). At Dongpan, increases in algal and acritarch abundance upsection within Beds 3 and 5 (i.e., below Bentonites 1 and 2; Fig. 5A) may indicate a modest stimulation of marine productivity, perhaps because of the

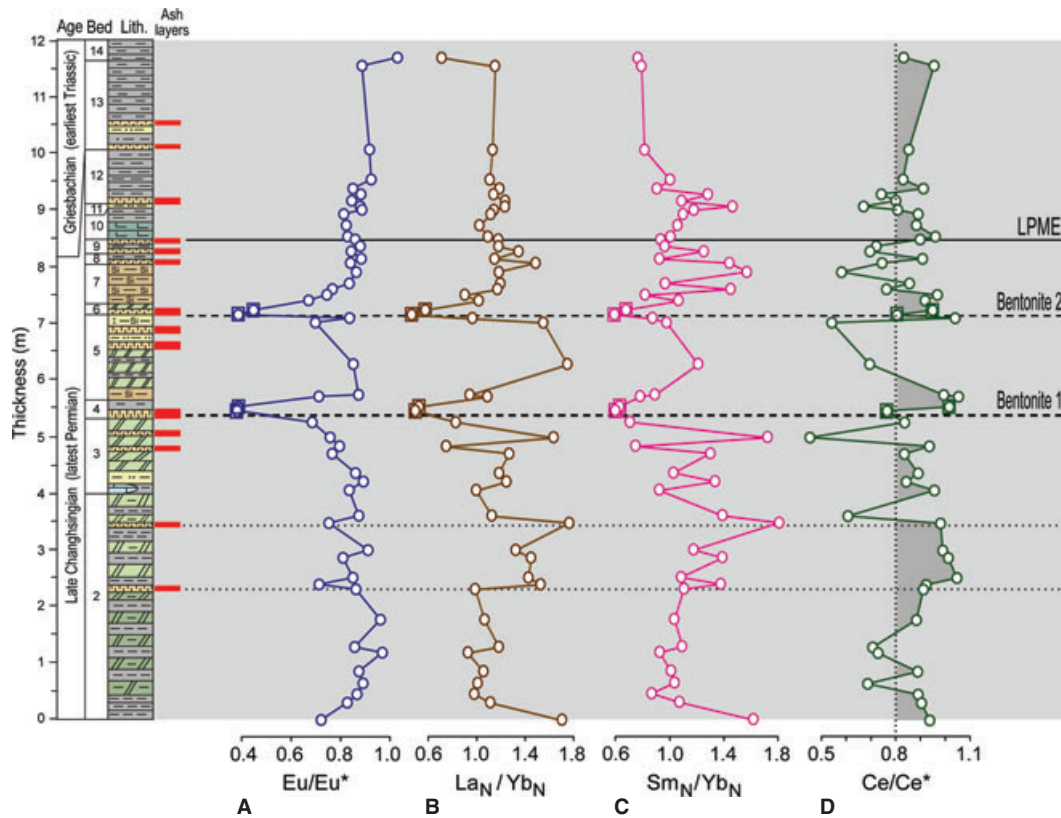


Fig. 8 REE chemostratigraphy: (A) Eu/Eu^* . (B) La_N/Yb_N . (C) Sm_N/Yb_N . (D) Ce/Ce^* . Eu/Eu^* and Ce/Ce^* were calculated per equations 5 and 6, and La_N/Yb_N and Sm_N/Yb_N are PAAS-normalized ratios representing LREE and MREE enrichment, respectively, relative to HREEs. Bentonites samples analyzed in this study are enclosed by squares. Dotted vertical line in D represents approximate division between oxic-suboxic conditions ($\text{Ce}/\text{Ce}^* < 0.8$) and anoxic conditions ($\text{Ce}/\text{Ce}^* > 0.8$; gray shading). Other features as in Fig. 3.

fertilization effects of subaerial weathering of volcanic materials (cf. Frogner *et al.*, 2001). Sharp declines in algal abundance just below Bentonites 1 and 2 as well as below the LPME (Fig. 5A) suggest that intensifying volcanic activity was ultimately detrimental to marine productivity, perhaps because of reduced light penetration, deposition of toxic metals, or acidification of surface waters by volcanic aerosols (Felixsyn & Kirianov, 2002; Sansone *et al.*, 2002). A decline in peak algal abundance from Bentonite 1 to Bentonite 2 and then to the LPME may reflect either an increase in eruption intensity for later volcanic cycles or the effects of accumulated stresses in the Dongpan marine environment with time.

Paleoproductivity potentially can be evaluated on the basis of excess Ba (Ba_{xs}), which develops as barite is precipitated on the surfaces of decaying organic particles in the water column when SO_4^{2-} from reoxidized H_2S encounters seawater Ba^{2+} (Dehairs *et al.*, 1992; Dymond *et al.*, 1992). High Ba_{xs} concentrations are common in sediments of high-productivity regions of the modern ocean (Murray & Leinen, 1993), but its use as a paleoproductivity proxy is complicated by influences on retention of Ba_{xs} in the sediment, for example, low concentrations of seawater sulfate, as inferred for the Late Permian–Early Triassic (Bottrell & Newton, 2006), can

reduce the stability of authigenic barite. Below the LPME at Dongpan, Ba_{xs} exhibits a stronger relationship to radiolarian abundance (Fig. 3) and biogenic SiO_2 (Fig. 5E) than to algal abundance (Fig. 5A), implying that Ba_{xs} was more closely related to zooplankton than to phytoplankton productivity. These relationships are logical given that most primary production in the modern ocean is consumed and reworked by zooplankton prior to export to the deep ocean (Calbet, 2001). A strong reduction in Ba_{xs} at the level of the LPME suggests that marine productivity declined considerably in response to this event.

Radiolarian communities

Radiolarians are single-celled marine eukaryotes that are one of the most conspicuous zooplankton clades inhabiting the modern pelagic ocean (Angel, 1991; Swanberg & Caron, 1991). They are generally present in high concentrations in the upper 100 m of the water column and more sporadically to depths of 1000 m (Ishitani *et al.*, 2008). Radiolarian orders exhibit specific depth preferences: Spumellaria and Entactinaria prefer shallower water, whereas Latentifistularia and (especially) Albaillellaria generally live in deeper water

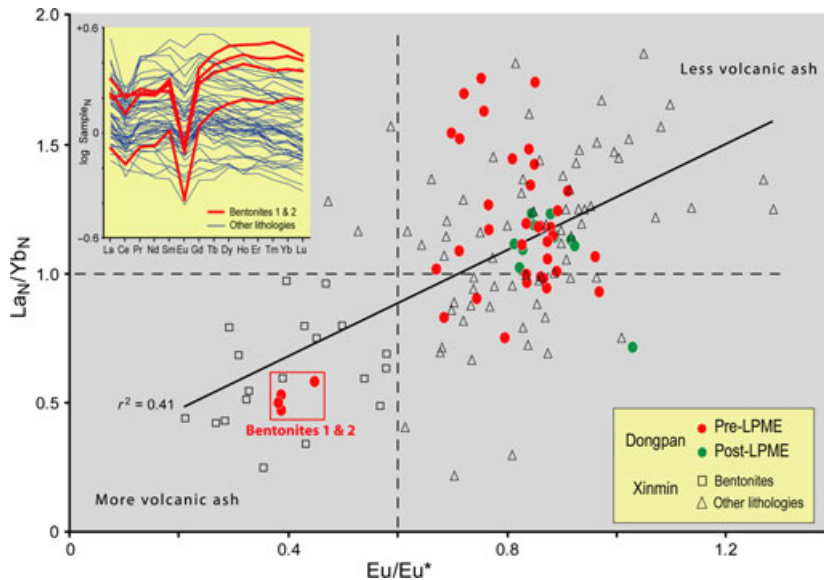


Fig. 9 Eu/Eu^* vs. La_N/Yb_N . Red and green symbols are pre-LPME and post-LPME samples from Dongpan, respectively; open triangles and squares are samples from bentonites and other lithologies of the Xinmin section, northern Guangxi Province (see Fig. 1 for location). Low Eu/Eu^* and La_N/Yb_N ratios are characteristic of volcanic ash layers in both sections, a relationship confirmed by the larger sample set from Xinmin (Shen *et al.*, in review).

(Kozur, 1993). Radiolarians are heterotrophs that feed on bacteria and algae using a pseudopodial net (Dennett *et al.*, 2002), but many colonial forms also harbor large numbers of symbiotic algae and dinoflagellates that contribute to the nutrition of the host (Caron *et al.*, 1995). Thus, radiolarian abundances in marine sediments may assist in assessing paleo-productivity levels owing to their dual roles as primary consumers dependent on phytoplankton biomass as well as hosts for symbiotic algae.

At Dongpan, the general upsection increase in radiolarian abundance to the level of Bentonite 2 may reflect a concurrent gradual rise in marine productivity (see Marine productivity). The subsequent rapid decline of radiolarians may have been caused either by a productivity crash (see Marine productivity) or by expansion of the OMZ within the Nanpanjiang Basin (see Marine redox conditions). Strong variations in radiolarian populations in other Upper Permian successions have been attributed to reduced nutrient availability linked to environmental disturbances or climate change (Kakuwa, 1996; Feng *et al.*, 2007; Isozaki *et al.*, 2007) or might be attributable to changes in trophic resources, for example, the decimation of eukaryotic algae and proliferation of green sulfur bacteria (Grice *et al.*, 2005; Knoll *et al.*, 2007; Cao *et al.*, 2009). However, extinction and survival patterns among different taxonomic orders support the hypothesis that a rising OMZ was the principal stress on radiolarian communities during the latest Permian: the order favoring the greatest water depths (*Albaillellaria*) went extinct, while among the surviving orders the relatively deepwater *Latentifistularia* fared more poorly than the shallower-water *Spumellaria* and *Entactinaria* (Fig. 3). Although lithologic and biotic changes within Beds

7–12 at Dongpan have been interpreted to reflect a pronounced eustatic shallowing event (He *et al.*, 2007), the shift from bathyal to neritic faunal assemblages instead may record an expansion of the OMZ (cf. Algeo *et al.*, 2010, 2011a) and consequent elimination of deeper-dwelling taxa.

Relationship of volcanic episodes to environmental and biotic changes

The volcanic episodes discussed in Volcanic episodes show a distinct relationship to the environmental proxies discussed in Terrestrial vegetation and wildfires, Marine redox conditions, Marine productivity, and Radiolarian communities, with changes in the various proxies occurring in nearly the same succession. Thus, the Bentonite 1 episode shows increases in algal-acritarch abundance beginning in the middle of Bed 3, and spore-pollen and charcoal abundance toward the top of Bed 3, followed by the main ash layer (Bed 4). The Bentonite 2 episode shows increases in algal-acritarch abundance beginning in the lower part of Bed 5, charcoal abundance in the middle of Bed 5, and spore-pollen abundance at the top of Bed 5, followed by the main ash layer (Bed 6). The only environmental variable for which changes do not occur prior to the main eruptive event is redox conditions, which tend to shift from oxic to anoxic concurrent with bentonite deposition. These relationships imply that systematic changes in the marine environment at Dongpan occurred in response to local volcanic activity and that such changes were underway prior to the main eruptive event in each episode.

One scenario that links volcanic activity with changes in terrestrial vegetation and marine environmental conditions is

based on the role of weathering fluxes. We infer that volcanic episodes triggered changes in terrestrial ecosystems (i.e., shifts toward greater conifer forest growth, more frequent wildfires) that led to an increased flux of eroded material into marine ecosystems. These fluxes included particulates (including volcanically derived clay minerals such as smectite and kaolinite), organic matter (including pollen, spores, and charcoal), and dissolved nutrients. The latter fraction initially stimulated marine productivity during each volcanic episode, resulting in increased concentrations of algae, acritarchs, and radiolarians. Higher levels of productivity resulted in greater respiratory oxygen demand at intermediate water depths, leading to an expansion of the OMZ within the Nanpanjiang Basin. OMZ expansion seems to have led to a negative feedback on marine productivity, resulting in declines in phytoplankton and zooplankton biomass. This pattern was repeated at least twice during the pre-LPME latest Permian, as recorded by the eruptive cycles of Bentonites 1 and 2.

The response of the marine environment at Dongpan to the disturbance represented by the LPME was in many respects similar to its response to the Bentonite 1 and 2 episodes. For example, algal-acritarch, spore-pollen, and charcoal abundances all increase within Bed 7 before declining within Beds 8 or 9, just below the LPME (Fig. 5), while the Ce/Ce* redox proxy shifts from oxic to anoxic at the LPME itself (Fig. 8D). Some proxies suggest that the environmental disturbances associated with the LPME were more severe than those during earlier volcanic episodes. For example, charcoal abundance is 3× to 5× greater than peak values below Bentonites 1 and 2 (Fig. 5C), suggesting a more intense destruction of terrestrial vegetation, and biogenic SiO₂ and Ba_{xs} exhibit larger and more sustained declines, suggesting greater declines in marine productivity and ecosystem disruption. Because the composition of the LPME contrasts with that of Bentonites 1 and 2 in lacking the signature of local volcanic inputs (e.g., kaolinite and low Eu/Eu* values; see Volcanic episodes), we infer that the LPME represents a disturbance of more distal origin, for example, the eruption of the Siberian Traps flood basalts (Reichow *et al.*, 2009). The Siberian Traps have been inferred to be associated with widespread destruction of terrestrial vegetation (Visscher *et al.*, 1996; Looy *et al.*, 2001) and consequent changes in organic and detrital weathering fluxes (Seph-ton *et al.*, 2005; Algeo & Twitchett, 2010).

CONCLUSIONS

High-resolution bio- and chemostratigraphic analyses of the Dongpan section in southern Guangxi Province, South China, provide new insights regarding marine environmental perturbations at intermediate water depths (~200–500 m) preceding the LPME. Although oxic conditions prevailed on the seafloor, episodic expansion of the OMZ higher in the water column of the Nanpanjiang Basin put planktonic communities under severe stress and resulted in declines in

primary productivity and in the diversity and abundance of the zooplankton (radiolarian) community. Marine conditions appear to have fluctuated in concert with those in surrounding terrestrial areas, both being controlled by volcanic episodes of local origin. Intensification of eruptive activity during each volcanic cycle appears to have resulted in a shift toward conifer forests, increased wildfire intensity, and elevated subaerial weathering fluxes that stimulated marine productivity in the short term. Higher sinking fluxes of organic matter then led to an expansion of the OMZ and a negative feedback on marine productivity. Radiolarians exhibit large declines in diversity and abundance well before the global LPME horizon, demonstrating the diachroneity of the latest Permian biotic crisis, at least within the Nanpanjiang Basin of South China. The LPME, which was probably triggered by the distant Siberian Traps flood basalts, had effects on marine and terrestrial environments of the South China craton that were similar to but more severe than those of earlier local volcanic eruptions.

ACKNOWLEDGMENTS

Thanks to Stephen Kershaw for editorial handling and anonymous reviewers for comments that improved the quality of this paper. We also send our thanks to Profs. Chaoyong Hu and Shucheng Xie for helpful discussions. This work was supported by NSFC (project no. 40839903, 40921062, 40972002 and 41073007), the 973 program (grant 2011CB808800), the 111 program (B08030), and the US National Science Foundation (grants EAR-0618003, -0745574, and -1053449 to TJA). This paper is a contribution to IGCP Project 572.

REFERENCES

- Albani R, Bagnoli G, Bernárdez E, Gutiérrez-Marco JC, Ribecai C (2006) Late Cambrian acritarchs from the “Túnel Ordovícico del Fabar”, Cantabrian Zone, N Spain. *Review of Palaeobotany and Palynology*, **139**, 41–52.
- Algeo TJ, Maynard JB (2004) Trace element behavior and redox facies in core shales of Upper Pennsylvanian Kansas-type cyclothems. *Chemical Geology*, **206**, 289–318.
- Algeo TJ, Twitchett R (2010) Anomalous Early Triassic sediment fluxes due to elevated weathering rates and their biological consequences. *Geology*, **38**, 1023–1026.
- Algeo TJ, Ellwood BB, Nguyen TKT, Rowe H, Maynard JB (2007a) The Permian-Triassic boundary at Nhi Tao, Vietnam: evidence for recurrent influx of sulfidic watermasses to a shallow-marine carbonate platform. *Palaeogeography Palaeoclimatology Palaeoecology*, **252**, 304–327.
- Algeo TJ, Hannigan R, Rowe H, Brookfield M, Baud A, Krystyn L, Ellwood BB (2007b) Sequencing events across the Permian-Triassic boundary, Guryul Ravine (Kashmir, India). *Palaeogeography Palaeoclimatology Palaeoecology*, **252**, 328–346.
- Algeo TJ, Shen YN, Zhang TG, Lyons T, Bates S, Rowe H, Nguyen TKT (2008) Association of ³⁴S-depleted pyrite layers with negative carbonate δ¹³C excursions at the Permian/Triassic boundary:

- evidence for upwelling of sulfidic deep-ocean watermasses. *Geochemistry Geophysics Geosystems*, **9**, Q04025, 10.
- Algeo TJ, Hinnov L, Moser J, Maynard JB, Elswick E, Kuwahara K, Sano H (2010) Changes in productivity and redox conditions in the Panthalassic Ocean during the latest Permian. *Geology*, **38**, 187–190.
- Algeo TJ, Kuwahara K, Sano H, Bates S, Lyons T, Elswick E, Hinnov L, Ellwood BB, Moser J, Maynard JB (2011a) Spatial variation in sediment fluxes, redox conditions, and productivity in the Permian-Triassic Panthalassic Ocean. *Palaeogeography Palaeoclimatology Palaeoecology*, **308**, 65–83.
- Algeo TJ, Chen ZQ, Fraiser ML, Twitchett RJ (2011b) Terrestrial-marine teleconnections in the collapse and rebuilding of Early Triassic marine ecosystems. *Palaeogeography Palaeoclimatology Palaeoecology*, **308**, 1–11.
- Alibo DS, Nozaki Y (1999) Rare earth elements in seawater: particle association, shale-normalization, and Ce oxidation. *Geochimica et Cosmochimica Acta*, **63**, 363–372.
- Aloy J, Aberhan M, Bottjer DJ, Foote M, Fürsich FT, Harries PJ, Hendy AJW, Holland SM, Ivany LC, Kiessling W, Kosnik MA, Marshall CR, MsGowan AJ, Miller AI, Olszewski TD, Patzkowsky ME, Peters SE, Villier L, Wagner PJ, Bonuso N, Borkow PS, Brenner B, Clapham ME, Fall LM, Ferguson CA, Hanson VL, Krug AZ, Layou KM, Leckey EH, Nurnberg S, Powers CM, Sessa JA, Simpson C, Tomašových A, Visaggi CC (2008) Phanerozoic trends in the global diversity of marine invertebrates. *Science*, **321**, 97–100.
- Angel DL (1991) Carbon flow within the colonial radiolarian microcosm. *Symbiosis*, **10**, 195–217.
- de Baar HJW, Brewer PG, Bacon MP (1985) Anomalies in rare earth distribution in seawater: Gd and Tb. *Geochimica et Cosmochimica Acta*, **49**, 1943–1959.
- Bottrell SH, Newton RJ (2006) Reconstruction of changes in global sulfur cycling from marine sulfate isotopes. *Earth-Science Reviews*, **75**, 59–83.
- Brenneke GA, Herrmann AD, Algeo TJ, Anbar AD (2011) Rapid expansion of oceanic anoxia immediately before the end-Permian mass extinction. *Proceedings of the National Academy of Sciences (USA)*, 4 pp. doi/10.1073/pnas.1106039108.
- Brown GE Jr, Parks GA (2002) Sorption of trace elements on mineral surfaces: modern perspectives from spectroscopic studies, and comments on sorption in the marine environment. In *Frontiers in Geochemistry: Organic, Solution, and Ore Deposit Geochemistry* (ed Ernst WG), Bellwether Publishing, Columbia, Maryland, 69–179.
- Calbet A (2001) Mesozooplankton grazing effect on primary production: a global comparative analysis in marine ecosystems. *Limnology and Oceanography*, **46**, 1824–1830.
- Cao CQ, Love GD, Hays LE, Wang W, Shen S, Summons RE (2009) Biogeochemical evidence for euxinic oceans and ecological disturbance presaging the end-Permian mass extinction event. *Earth and Planetary Science Letters*, **281**, 188–201.
- Caron DA, Michaels AF, Swanberg NR, Howse FA (1995) Primary productivity by symbiont-bearing planktonic sarcodines (Acantharia, Radiolaria, Foraminifera) in surface waters near Bermuda. *Journal of Plankton Research*, **17**, 103–129.
- Chamley H (1989) *Clay Mineralogy*. Springer, Berlin, 623 pp.
- CRC (2004) *Handbook of Physics and Chemistry, 85th edn*, CRC Press, Boca Raton, Florida.
- De Wit MJ, Ghosh JG, de Villiers S, Rakotosolofa N, Alexander J, Tripathi A, Looy C (2002) Multiple organic carbon isotope reversals across the Permo-Triassic boundary of terrestrial Gondwana sequences: clues to extinction patterns and delayed ecosystem recovery. *Journal of Geology*, **110**, 227–240.
- Dehairs F, Baeyens W, Goeyens L (1992) Accumulation of suspended barite at mesopelagic depths and export production in the Southern Ocean. *Science*, **258**, 1332–1335.
- Dennett MR, Caron DA, Michaels AF, Gallager SM, Davis CS (2002) Video plankton recorder reveals high abundances of colonial Radiolaria in surface waters of the central North Pacific. *Journal of Plankton Research*, **24**, 797–805.
- Dymond JR, Suess E, Lyle M (1992) Barium in deep-sea sediment: a geochemical proxy for paleoproductivity. *Paleoceanography*, **7**, 163–181.
- Elderfield H (1988) The oceanic chemistry of the rare-earth elements. *Philosophical Transactions of the Royal Society of London*, **325**, 105–126.
- Elderfield H, Greaves MJ (1982) The rare earth elements in seawater. *Nature*, **296**, 214–219.
- Ellwood BB, Crick RE, El Hassani A, Benoist S, Young RH (2000) Magnetosusceptibility event and cyclostratigraphy method applied to marine rocks: detrital input versus carbonate productivity. *Geology*, **28**, 1135–1138.
- Ellwood BB, Tomkin JK, Ratcliffe KT, Wright M, Kafafy AM (2008) High-resolution magnetic susceptibility and geochemistry for the Cenomanian/Turonian boundary GSSP with correlation to time equivalent core. *Palaeogeography Palaeoclimatology Palaeoecology*, **26**, 105–126.
- Ellwood BB, Algeo TJ, El Hassani A, Tomkind JH, Rowe HD (2011) Defining the timing and duration of the Kačák Interval within the Eifelian/Givetian boundary GSSP, Mech Irdane, Morocco, using geochemical and magnetic susceptibility patterns. *Palaeogeography Palaeoclimatology Palaeoecology*, **304**, 74–84.
- Erwin DH, Bowring SA, Jin YG (2002) End-Permian mass-extinctions: A review. In *Catastrophic Events and Mass Extinctions: Impacts and Beyond* (eds Koeberl C, MacLeod KG). Geological Society of America Special Paper, 356, Boulder, Colorado, pp. 353–383.
- Felitsyn SB, Kirianov VY (2002) Mobility of phosphorus during the weathering of volcanic ashes. *Lithology and Mineral Resources*, **37**, 275–278.
- Feng QL, Gu SZ (2002) Uppermost Changxingian (Permian) radiolarian fauna from southern Guizhou, southwestern China. *Journal of Paleontology*, **76**, 797–809.
- Feng QL, Yang FQ, Zhang ZF, Gao YQ, Wang ZP (2000) Radiolarian evolution during the Permian and Triassic transition in South and Southwest China. In *Permian-Triassic Evolution of Tethys and Western Circum-Pacific* (eds Yin H, Dickens JH, Shi GR, Tong J), Elsevier, Amsterdam, 309–326.
- Feng QL, He WH, Gu SZ, Meng YY, Jin YX, Zhang F (2007) Radiolarian evolution during the latest Permian in South China. *Global and Planetary Change*, **55**, 177–192.
- Frogner P, Gíslason SR, Oskarsson N (2001) Fertilizing potential of volcanic ash in ocean surface water. *Geology*, **29**, 487–490.
- German CR, Elderfield H (1990) Application of the Ce anomaly as a paleoredox indicator: the ground rules. *Paleoceanography*, **5**, 823–833.
- Grasby SE, Beauchamp B (2009) Latest Permian to Early Triassic basin-to-shelf anoxia in the Sverdrup Basin, Arctic Canada. *Chemical Geology*, **264**, 232–246.
- Grice K, Cao CQ, Love GD, Böttcher ME, Twitchett RJ, Grosjean E, Summons RE, Turgeon SC, Dunning W, Jin YG (2005) Photic zone euxinia during the Permian-Triassic superanoxic event. *Science*, **307**, 706–709.
- Guo Y, Bustin RM (1998) FTIR spectroscopy and reflectance of modern charcoals and fungal decayed woods: implications for studies of inertinite in coals. *International Journal of Coal Geology*, **37**, 29–53.

- He WH, Shen SZ, Feng QL, Gu SZ (2005a) A Late Changhsingian (Late Permian) deepwater brachiopod fauna from the Talung Formation at the Dongpan section, southern Guangxi, South China. *Journal of Paleontology*, **79**, 927–938.
- He WH, Feng QL, Gu SZ, Jin YX (2005b) Changxingian (Upper Permian) radiolarian fauna from Meishan D section, Changxing, Zhejiang, China and its possible paleoecological significance. *Journal of Paleontology*, **79**, 209–218.
- He WH, Shi GR, Feng QL, Campi MJ, Gu SZ, Bu JJ, Peng YQ, Meng YY (2007) Brachiopod miniaturization and its possible causes during the Permian-Triassic crisis in deep water environments, South China. *Palaeogeography Palaeoclimatology Paleocology*, **252**, 145–163.
- Hunt JM (1996) *Petroleum Geochemistry and Geology*, 2nd edn. W.H. Freeman, New York, 743 pp.
- Ishitani Y, Takahashi K, Okazaki Y, Tanaka S (2008) Vertical and geographic distribution of selected radiolarian species in the North Pacific. *Micropaleontology*, **54**, 27–39.
- Isozaki Y (1997) Permo-Triassic boundary superanoxia and stratified superocean; records from lost deep sea. *Science*, **276**, 235–238.
- Isozaki Y, Shimizu N, Yao J, Ji Z, Matsuda T (2007) End-Permian extinction and volcanism-induced environmental stress: the Permian-Triassic boundary interval of lower-slope facies at Chaotian, South China. *Palaeogeography Palaeoclimatology Paleocology*, **252**, 218–238.
- Jin YG, Wang Y, Wang W, Shang QH, Cao CQ, Erwin DH (2000) Pattern of marine mass extinction near the Permian Triassic boundary in South China. *Science*, **289**, 432–436.
- Kakuwa Y (1996) Permian-Triassic mass extinction event recorded in bedded chert sequence in southwest Japan. *Palaeogeography Palaeoclimatology Paleocology*, **121**, 35–51.
- Kakuwa Y, Matsumoto R (2006) Cerium negative anomaly just before the Permian and Triassic boundary event—the upward expansion of anoxia in the water column. *Palaeogeography Palaeoclimatology Paleocology*, **229**, 335–344.
- Kato Y, Nakao K, Isozaki Y (2002) Geochemistry of Late Permian to Early Triassic pelagic cherts from southwest Japan: implications for an oceanic redox change. *Chemical Geology*, **182**, 15–34.
- Kiehl JT, Shields CA (2005) Climate simulation of the latest Permian: implications for mass extinction. *Geology*, **33**, 757–760.
- Knoll AH, Bambach RK, Payne JL, Pruss S, Fischer WW (2007) Paleophysiology and end-Permian mass extinction. *Earth and Planetary Science Letters*, **256**, 295–313.
- Kozur HW (1993) Upper Permian radiolarians from the Sosio Valley Area, western Sicily (Italy) and from the uppermost Lamar Limestone of West Texas. *Jahrbuch der Geologischen Bundesanstalt Wien*, **136**, 99–123.
- Kump LR, Pavlov A, Arthur MA (2005) Massive release of hydrogen sulfide to the surface ocean and atmosphere during intervals of oceanic anoxia. *Geology*, **33**, 397–400.
- Kuwahara K, Yao A, Yamakita S (1998) Reexamination of Upper Permian radiolarian biostratigraphy. *Chikyu Kagaku* (“*Earth Science*”), **52**, 391–404. (in Japanese).
- Lécuyer C, Reynard B, Grandjean P (2004) Rare earth element evolution of Phanerozoic seawater recorded in biogenic apatites. *Chemical Geology*, **204**, 63–102.
- Li ZB (1989) Research on the maturity of organic matter and its controlling factors in the Upper Permian of the Nanpanjiang Basin. *Yunnan Geology*, **8**, 48–57. (in Chinese).
- Li ZX (1998) Tectonic history of the major East Asian lithospheric blocks since the mid-Proterozoic—A synthesis. In *Mantle Dynamics and Plate Interactions in East Asia* (eds Flower MFJ, Chung SL, Lo CH, Lee TY). Am. Geophys. Union Geodynamics Ser. 27, Washington, DC, pp. 221–243.
- Looy CV, Twitchett RJ, Dilcher DL, van Konijnenburg-van Cittert JHA, Visscher H (2001) Life in the end-Permian dead zone. *Proceedings of the National Academy of Sciences of the USA*, **98**, 7879–7883.
- Luo GM, Lai XL, Feng QL, Jiang HS, Wignall P, Zhang KX, Sun YD, Wu J (2008) End-Permian conodont fauna from Dongpan section: correlation between the deep- and shallow-water facies. *Science in China Series D: Earth Science*, **51**, 1611–1622.
- Luo GM, Wang Y, Yang H, Algeo TJ, Kump LR, Huang J, Xie SC (2011) Stepwise and large-magnitude negative shift in $\delta^{13}\text{C}_{\text{carb}}$ preceded the main marine mass extinction of the Permian-Triassic crisis interval. *Palaeogeography Palaeoclimatology Paleocology*, **299**, 70–82.
- Lyons TW, Severmann S (2006) A critical look at iron paleoredox proxies: new insights from modern euxinic marine basins. *Geochimica et Cosmochimica Acta*, **70**, 5698–5722.
- Maliva RG, Dickson JAD, Fallick AE (1999) Kaolin cements in limestones; potential indicators of organic-rich pore waters during diagenesis. *Journal of Sedimentary Research*, **69**, 158–163.
- McLennan SM (2001) Relationships between the trace element composition of sedimentary rocks and upper continental crust. *Geochemistry Geophysics Geosystems*, **2**, GC000109, 24 pp.
- Meng YY, Feng QL, He WH (2005) A unique deep-water Permian-Triassic boundary section from the Liuqiao region in southwestern Guangxi, South China. *Journal of Stratigraphy*, **29**, 323–332 (in Chinese).
- Millot G (1970) *Geology of Clays*. Springer, Berlin, 425 pp.
- Murray RW, Leinen M (1993) Chemical transport to the seafloor of the equatorial Pacific Ocean across a latitudinal transect at 135W: tracking sedimentary major, trace, and rare earth element fluxes at the Equator and the Intertropical Convergence Zone. *Geochimica et Cosmochimica Acta*, **57**, 4141–4163.
- Musashino M (1990) The Panthalassa—a cerium-rich Atlantic-type ocean: sedimentary environments of the Tamba Group, Southwest Japan. *Tectonophysics*, **181**, 165–177.
- Nielsen JK, Shen Y (2004) Evidence for sulfidic deep water during the Late Permian in the East Greenland Basin. *Geology*, **32**, 1037–1040.
- Nozaki Y, Alibo DS (2003) Importance of vertical geochemical processes in controlling the oceanic profiles of dissolved rare earth elements in the northeastern Indian Ocean. *Earth and Planetary Science Letters*, **205**, 155–172.
- Payne J, van de Schootbrugge B (2007) Life in Triassic oceans: links between benthic and planktonic recovery and radiation. In *The Evolution of Primary Producers in the Sea* (eds Falkowski PG, Knoll AH), Academic Press, New York, 165–189.
- Peng YQ, Tong JN, Shi GR, Hansen HJ (2001) The Permian-Triassic boundary stratigraphic set: characteristics and correlation. *Newsletters on Stratigraphy*, **39**, 55–71.
- Pessagno EA Jr, Newport RL (1972) A technique for extracting Radiolaria from radiolarian cherts. *Micropaleontology*, **18**, 231–234.
- Price JR, Velbel MA (2003) Chemical weathering indices applied to weathering profiles developed on heterogeneous felsic metamorphic parent rocks. *Chemical Geology*, **202**, 397–416.
- Rampino MR, Prokoph A, Adler A (2000) Tempo of the end-Permian event: high-resolution cyclostratigraphy at the Permian-Triassic boundary. *Geology*, **28**, 643–646.
- Reichow MK, Pringle MS, Al'Mukhamedov AI, Allen MB, Andreichev VL, Buslov MM, Davies CE, Fedoseev GS, Fitton JG, Inger S, Medvedev AY, Mitchell C, Puchkov VN, Safanova IY, Scott RA, Saunders AD (2009) The timing and extent of the eruption of the Siberian Traps large igneous province: Implications for the end-Permian environmental crisis. *Earth and Planetary Science Letters*, **277**, 9–20.

- Riccardi AL, Arthur MA, Kump LR (2006) Sulfur isotopic evidence for chemocline upward excursions during the end-Permian mass extinction. *Geochimica et Cosmochimica Acta*, **70**, 5740–5752.
- Sansone FJ, Benitez-Nelson CR, Resing JA, DeCarlo EH, Vink SM, Heath JA, Huebert BJ (2002) Geochemistry of atmospheric aerosols generated from lava-seawater interactions. *Geophysical Research Letters*, **29**, 1335–1338.
- Scott AC (1989) Observations on the nature and origin of fusain. *International Journal of Coal Geology*, **12**, 443–475.
- Sephton MA, Looy CV, Brinkhuis H, Wignall PB, de Leeuw JW, Visscher H (2005) Catastrophic soil erosion during the end-Permian biotic crisis. *Geology*, **33**, 941–944.
- Shen J, Algeo TJ, Hu Q, Xu G, Zhou L, Feng Q (in review) Volcanism in South China during the Late Permian and its relationship to marine ecosystem and environmental changes. *Global and Planetary Change*.
- Sholkovitz ER (1992) Chemical evolution of rare earth elements: fractionation between colloidal and solution phases of filtered river water. *Earth and Planetary Science Letters*, **114**, 77–84.
- Sholkovitz ER, Landing WM, Lewis BL (1994) Ocean particle chemistry: the fractionation of rare earth elements between suspended particles and seawater. *Geochimica et Cosmochimica Acta*, **58**, 1567–1579.
- Sholkovitz ER, Elderfield H, Szymczak R, Casey K (1999) Island weathering: river sources of rare earth elements to the Western Pacific Ocean. *Marine Chemistry*, **68**, 39–57.
- Staub JR, Cohen AD (1978) Kaolinite-enrichment beneath coals, a modern analog, Snuggedy Swamp, South Carolina. *Journal of Sedimentary Petrology*, **48**, 203–210.
- Sutton SJ, Maynard JB (1993) Sediment- and basalt-hosted regoliths in the Huronian supergroup: role of parent lithology in middle Precambrian weathering profiles. *Canadian Journal of Earth Science*, **30**, 60–76.
- Swanberg NR, Caron DA (1991) Patterns of sardine feeding in epipelagic oceanic plankton. *Journal of Plankton Research*, **13**, 287–312.
- Swartzendruber LJ (1992) Properties, units and constants in magnetism. *Journal of Magnetic Materials*, **100**, 573–575.
- Takahashi S, Yamakita S, Suzuki N, Kaiho K, Ehiro M (2009) High organic carbon content and a decrease in radiolarians at the end of the Permian in a newly discovered continuous pelagic section: a coincidence? *Palaeogeography Palaeoclimatology Palaeoecology*, **271**, 1–12.
- Taylor SR, McLennan SM (1985) *The Continental Crust: Its Composition and Evolution*. Blackwell, Oxford, 312 pp.
- Tinus RW, Roddy DJ (1990) Effects of global atmospheric perturbations on forest ecosystems in the Northern Temperate Zone; Predictions of seasonal depressed-temperature kill mechanisms, biomass production, and wildfire soot emissions. In: *Global Catastrophes in Earth History* (eds Sharpton VL, Ward PD). Geological Society of America Special Paper 247, Boulder, Colorado, pp. 77–86.
- Tong JN, Zhang SX, Zuo JX, Xiong XQ (2007) Events during Early Triassic recovery from the end-Permian extinction. *Global and Planetary Change*, **55**, 66–80.
- Tribouillard N, Algeo TJ, Lyons TW, Riboulleau A (2006) Application of trace metals as paleoredox and paleoproductivity proxies. *Chemical Geology*, **232**, 12–32.
- Visscher H, Brinkhuis H, Dilcher DL, Eshet Y, Looy CV, Rampino MR, Traverse A (1996) The terminal Paleozoic fungal event: evidence of terrestrial ecosystem destabilization and collapse. *Proceedings of the National Academy of Sciences of the USA*, **93**, 2155–2158.
- Wignall PB, Newton R (2003) Contrasting deep-water records from the Upper Permian and Lower Triassic of South Tibet and British Columbia: evidence for a diachronous mass extinction. *Palaaios*, **18**, 153–167.
- Winguth AME, Maier-Reimer E (2005) Causes of marine productivity and oxygen changes associated with the Permian-Triassic boundary: a reevaluation with ocean general circulation models. *Marine Geology*, **217**, 283–304.
- Xia W, Zhang N, Wang G, Kakuwa Y (2004) Pelagic radiolarian and conodont biozonation in the Permo-Triassic boundary interval and correlation to the Meishan GSSP. *Micropaleontology*, **50**, 27–44.
- Xie SC, Pancost RD, Wang Y, Yang H, Wignall PB, Luo GM, Jia CL, Chen L (2010) Cyanobacterial blooms tied to volcanism during the 5 m.y. Permo-Triassic biotic crisis. *Geology*, **38**, 447–450.
- Xie SC, Pancost RD, Yin HF, Wang HM, Evershed RP (2005) Two episodes of microbial change coupled with Permo/Triassic faunal mass extinction. *Nature*, **434**, 494–497.
- Yang K (1998) A plate reconstruction of the Eastern Tethyan Orogen in southwestern China. In *Mantle Dynamics and Plate Interactions in East Asia* (eds Flower MFJ, Chung SL, Lo CH, Lee TY). Am. Geophys. Union Geodynamics Ser. 27, Washington, DC, pp. 269–287.
- Yang ZY, Yin HF, Wu SB (1987) *Permian-Triassic Boundary Stratigraphy and Fauna of South China*. Geological Publishing House, Beijing, 32 pp.
- Yin H, Huang S, Zhang K, Hansen HJ, Yang F, Ding M, Bie X (1992) The effects of volcanism on the Permo-Triassic mass extinction in South China. In *Permo-Triassic Events in the Eastern Tethys: Stratigraphy, Classification, and Correlation with the Western Tethys* (eds Sweet WC, Yang Z, Dickins JM, Yin H), Cambridge U. Press, Cambridge, 146–157.
- Yin HF, Zhang KX, Tong JN, Yang ZY, Wu SB (2001) The global stratotype section and point (GSSP) of the Permian-Triassic boundary. *Episodes*, **24**, 102–114.
- Yin HF, Feng QL, Lai XL, Baud A, Tong JN (2007) The protracted Permo-Triassic crisis and multi-episode extinction around the Permian-Triassic boundary. *Global and Planetary Change*, **55**, 1–20.
- Zhang F, Feng QL, Meng YY, He WH, Gu SZ (2006) Stratigraphy of organic carbon isotope and associated events across the Permian and Triassic boundary in the Dongpan deepwater section in Liugia area, Guangxi, South China. *Geoscience*, **20**, 42–48.
- Zhang F, Feng QL, He WF, Meng YY, Gu SZ (2007) Multidisciplinary stratigraphic correlation of the Permian-Triassic boundary between the Dongpan deep-water environment section and the Guangxi and Meishan sections. *Geological Science and Technology Information*, **26**, 41–45 (in Chinese).
- Zhong H, Zhu WG, Chu ZY, He DF, Song XY (2007) Shrimp U–Pb zircon geochronology, geochemistry, and Nd–Sr isotopic study of contrasting granites in the Emeishan large igneous province, SW China. *Chemical Geology*, **236**, 112–133.
- Zhou MF, Robinson PT, Leshner CM, Keays RR, Zhang CJ, Malpas J (2005) Geochemistry, petrogenesis and metallogenesis of the Panzhihua Gabbroic Layered Intrusion and associated Fe–Ti–V oxide deposits, Sichuan Province, SW China. *Journal of Petrology*, **46**, 2253–2280.